MOLECULAR ECOLOGY

Globally-distributed microbial eukaryotes exhibit endemism at deep-sea hydrothermal vents

Journal:	*Molecular Ecology*
Manuscript ID	MEC-22-0728.R1
Manuscript Type:	Special Issue
Date Submitted by the Author:	n/a
Complete List of Authors:	Hu, Sarah; Woods Hole Oceanographic Institution, Marine Chemistry & Geochemistry Smith, Amy; Woods Hole Oceanographic Institution, Marine Chemistry & Geochemistry; Bard College at Simon's Rock Anderson, Rika; Carleton College, Biology Department Sylva, Sean; Woods Hole Oceanographic Institution, Marine Chemistry & Geochemistry Setzer, Michaela; University of Hawai'i at Mānoa Pacific Biosciences Research Center, Kewalo Marine Laboratory; University of Hawai'i at Mānoa, Department of Oceanography Steadmon, Maria; University of Hawai'i at Mānoa Pacific Biosciences Research Center, Kewalo Marine Laboratory; University of Hawai'i at Mānoa, Department of Oceanography Frank, Kiana; University of Hawai'i at Mānoa Pacific Biosciences Research Center, Kewalo Marine Laboratory Chan, Eric; The University of Texas Rio Grande Valley - Edinburg Campus, School of Earth, Environmental, and Marine Sciences Lim, Darlene; NASA Ames Research Center German, Chris; Woods Hole Oceanographic Institution, Department of Geology & Geophysics Breier, John; The University of Texas Rio Grande Valley - Edinburg Campus, School of Earth, Environmental, and Marine Sciences Lang, Susan; Woods Hole Oceanographic Institution, Department of Geology & Geophysics; University of South Carolina, School of the Earth, Ocean, and Environment Butterfield, David; University of Washington, Joint Institute for the Study of Atmosphere and Ocean Fortunato, Caroline; Widener University, Department of Biology Seewald, Jeffrey; Woods Hole Oceanographic Institution, Marine Chemistry & Geochemistry Huber, Julie; Woods Hole Oceanographic Institution, Marine Chemistry & Geochemistry
Keywords:	Protists, hydrothermal vent, DNA Barcoding, Microbial diversity, Microbial eukaryotes

Globally-distributed microbial eukaryotes exhibit endemism at deep-sea hydrothermal vents

Sarah K. Hu[1*], Amy R. Smith[1,2], Rika E. Anderson[3], Sean P. Sylva[1], Michaela Setzer[4,5], Maria Steadmon[4,5], Kiana L. Frank[4], Eric W. Chan[8], Darlene S. S. Lim[6], Christopher R. German[7], John A. Breier[8], Susan Q. Lang[7,9], David A. Butterfield[10], Caroline S. Fortunato[11], Jeffrey S. Seewald[1], & Julie A. Huber[1]

[1] Department of Marine Chemistry and Geochemistry, Woods Hole Oceanographic Institution, Woods Hole, MA 02543, USA
[2] Bard College at Simon's Rock, Great Barrington, MA 01230, USA
[3] Biology Department, Carleton College, Northfield, MN 55057, USA
[4] Pacific Biosciences Research Center, Kewalo Marine Laboratory, University of Hawai'i at Mānoa, Honolulu, HI 96813, USA
[5] Department of Oceanography, University of Hawaii at Mānoa, Honolulu, HI, 96822, USA
[6] NASA Ames Research Center, Mountain View, CA 94035, USA
[7] Department of Geology & Geophysics, Woods Hole Oceanographic Institution, Woods Hole, MA 02543, USA
[8] School of Earth, Environmental, and Marine Sciences, The University of Texas Rio Grande Valley, Edinburg, TX 78539, USA
[9] School of the Earth, Ocean, and Environment, University of South Carolina, Columbia, SC 29208, USA
[10] Joint Institute for the Study of Atmosphere and Ocean, University of Washington, Seattle, WA 98195, USA
[11] Department of Biology, Widener University, Chester, PA 19013 USA

*Corresponding Author, sarah.hu@whoi.edu

Running title: Hydrothermal vent microbial eukaryotes

Conflict of interest: Authors declare no conflict of interest.

Key words: deep-sea hydrothermal vent, microbial diversity, protistan diversity, microbial eukaryotes, hydrothermal vent food web

ABSTRACT

Single-celled microbial eukaryotes inhabit deep-sea hydrothermal vent environments and play critical ecological roles in the vent-associated microbial food web. 18S rRNA amplicon sequencing of diffuse venting fluids from four geographically- and geochemically-distinct hydrothermal vent fields was applied to investigate community diversity patterns among protistan assemblages. The four vent fields include Axial Seamount at the Juan de Fuca Ridge, Sea Cliff and Apollo at the Gorda Ridge, all in the NE Pacific Ocean, and Piccard and Von Damm at the Mid-Cayman Rise in the Caribbean Sea. We describe species diversity patterns with respect to hydrothermal vent field and sample type, identify putative vent endemic microbial eukaryotes, and test how vent fluid geochemistry may influence microbial community diversity. At a semi-global scale, microbial eukaryotic communities at deep-sea vents were composed of similar proportions of dinoflagellates, ciliates, Rhizaria, and stramenopiles. Individual vent fields supported distinct and highly diverse assemblages of protists that included potentially endemic or novel vent-associated strains. These findings represent a census of deep-sea hydrothermal vent protistan communities. Protistan diversity, which is shaped by the hydrothermal vent environment at a local scale, ultimately influences the vent-associated microbial food web and the broader deep-sea carbon cycle.

1. INTRODUCTION

Deep-sea hydrothermal vent habitats are biological hotspots in the dark ocean, where a rich food web is fueled by chemosynthetic microorganisms (Huber *et al.*, 2007; Bennett *et al.*, 2013; McNichol *et al.*, 2018). The composition of microbial communities at deep-sea hydrothermal vents is influenced by vent fluid chemistry, temperature, prey availability, and geological setting; as a result, individual sites of venting fluid within the same vent field may host distinct microbial communities (Huber *et al.*, 2006; Opatkiewicz *et al.*, 2009; Akerman *et al.*, 2013; Fortunato *et al.*, 2018). Accordingly, constraining how these parameters drive both the prokaryotic and eukaryotic microbial diversity and community structure is key to understanding hydrothermal vent food web ecology (Sievert and Vetriani, 2012; Bell *et al.*, 2017). Documenting microbial biogeography across spatial and temporal gradients is also important for assessing how selective or disruptive processes influence microbial community structure.

Unicellular microbial eukaryotes (referred to as protists) fulfill critical ecological roles in marine food webs and form highly diverse community assemblages at deep-sea niche habitats, such as hydrothermal vents (Edgcomb *et al.*, 2002; López-García *et al.*, 2003, 2007; Sauvadet *et al.*, 2010; Murdock and Juniper, 2019). Culture and microscopy-based studies have also demonstrated that deep-sea protists thrive in extreme environments where they may encounter a wide range of temperatures and/or pressures, as well as be exposed to high concentrations of dissolved sulfide and metals, all of which can impact their life cycle (Small and Gross, 1985; Atkins *et al.*, 1998, 2000; Baumgartner *et al.*, 2002; Živaljić *et al.*, 2020). Consistent with bacterial and archaeal diversity associated with hydrothermal vent habitats, genetic studies have found protistan assemblages within diffuse vent fluids to be more species-rich compared to the

surrounding deep seawater (Murdock and Juniper, 2019; Hu *et al.*, 2021), and they may form distinct community assemblages at distances of only tens of centimeters (Pasulka *et al.*, 2019). Along with this trend in diversity, protistan grazers (or heterotrophic predators of microbes) place greater predation pressure on the vent-associated microbial population compared to the surrounding deep seawater (Hu *et al.*, 2021). Protistan community diversity and distribution therefore has implications for how carbon is exchanged and exported in deep-sea microbial food webs (Sauvadet *et al.*, 2010).

Here, we applied amplicon tag-sequencing to address three core questions, (1) What is the biogeography and distribution of the deep-sea hydrothermal vent microbial eukaryotic community?, (2) Are characteristic features of protistan community structure (*i.e.,* species richness, endemic vs. widely distributed) shared across or unique to separate hydrothermal vent fields?, and (3) What biotic or abiotic parameters appear to influence protistan community diversity at deep-sea hydrothermal vents? And do specific environmental parameters select for putative vent endemic protists? Our findings shed new light on the distribution of microbial eukaryotes at deep-sea hydrothermal vents globally and explore how fluid geochemistry and geography influence vent-associated protistan assemblages.

2. MATERIALS & METHODS

2.1. Collection of samples for molecular biology & geochemistry

Samples were derived from a total of 5 different research expeditions. Axial Seamount samples were obtained across 4 cruises in 3 years: in 2013 from the RV Falkor (FK010) and RV Thomas G. Thompson (TN300), in 2014 on NOAA Ship Ronald H. Brown (RB1403), and in 2015 on the RV Thomas G. Thompson (TN327). Samples from the Gorda Ridge were obtained in 2019 on the EV Nautilus (NA-108) and samples from the Mid-Cayman Rise were collected on the RV Atlantis (AT42-22) in 2020. Descriptions of cruise methods, library preparation, and processing are also available at BCO-DMO (https://www.bco-dmo.org/project/818746).

Samples from Axial Seamount cover a 3-year time series (2013-2015) (Table S1; Topçuoğlu *et al.*, 2016; Fortunato *et al.*, 2018), where 2015 samples were collected months after an eruption (Spietz *et al.*, 2018; Baker *et al.*, 2019). Each year, samples from several vent sites within Axial Seamount were collected and in 2015, fluid from the water column plume (42 m above Anemone vent) and background seawater (1500 m water depth) were also obtained (also see Fortunato *et al.*, 2018). Using ROVs ROPOS and Jason, 3 L of diffuse hydrothermal vent fluid was pumped through a 47 mm diameter GWSP (mixed cellulose esters; MCE) filter (Millipore) with a pore size of 0.22 µm using the Hydrothermal Fluid and Particle Sampler (HFPS; Butterfield *et al.*, 2004). Plume and background seawater was collected using a 10 L Niskin bottle. All filters were preserved *in situ* with RNALater (Ambion) as previously described in Akerman *et al.* (2013). Collection of geochemical parameters from Axial Seamount are described in Fortunato *et al.* (2018), where samples were analyzed for methane, magnesium, dissolved hydrogen gas, and

hydrogen sulfide using methods described in Butterfield *et al.* (2004). pH was measured *in situ* using a deep-sea glass pH electrode (AMT) plumbed to the HFPS.

South from Axial Seamount are the Sea Cliff and Apollo hydrothermal vent fields (~2700 m depth) along the basalt-hosted Gorda Ridge spreading center (~200 km off the coast of southern Oregon). Four sites of diffuse venting fluid were targeted within the Sea Cliff and Apollo vent fields, which included Venti Latte, Mt. Edwards, Candelabra, and Sir Ventsalot; samples from Gorda Ridge included in this study are from Hu *et al.* (2021). Low-temperature diffuse fluid (selected using a temperature probe mounted on the sampler intake) was collected by pumping 4.1-6.6 L of fluid through a 142 mm diameter 0.2 µm pore size polyethersulfone (PES) filter (Millipore) with the Suspended Particulate Rosette sampler (SUPR; Breier *et al.*, 2014) mounted on ROV Hercules. Once shipboard, filters were stored and frozen in RNALater. Niskin bottles mounted on the port side of the ROV were used to sample plume (~5 m above active venting) and background seawater environments; seawater from Niskins was transferred into acid-rinsed and clean cubitainers, filtered through 0.2 µm Sterivex filters (Millipore), and preserved with RNALater. In addition to samples collected meters above diffuse venting fluid at Mt. Edwards and Candelabra (respective plumes), a sample was collected laterally from diffuse fluid (deemed Near Vent BW), but was distinct from background seawater.

In the Western Caribbean, the Mid-Cayman Rise is an ultraslow spreading ridge that includes two geologically-distinct vent fields approximately 20 km apart: Piccard (~4950 m) and Von Damm (~2350 m). Vent fluids from Piccard are typically acidic and enriched in dissolved sulfide and hydrogen, as fluid exiting the seafloor interacts with mafic rock. In contrast, vent fluid from

Von Damm is influenced by ultramafic rock, resulting in less acidic fluid with comparatively less dissolved sulfide (Table 1). In total, 2 sites of low temperature diffuse venting fluid were sampled at Piccard and 8 vent sites were sampled at Von Damm using the Hydrothermal Organic Geochemistry sampler (HOG; Lang and Benitez-Nelson, 2021) mounted on ROV Jason. Between 4-10 L of vent fluid was filtered through a 47 mm polyethersulfone (PES) filter (Millipore) with a pore size of 0.2 µm. Similar to samples from Axial Seamount, *in situ* filters were preserved in RNALater at the seafloor, as described in Akerman *et al.* (2013). 12 L Niskin bottles collected deep seawater and plume samples at both Von Damm and Piccard. Seawater obtained via Niskin bottle was collected into acid-rinsed and clean carboys and filtered onto Sterivex filters (Millipore) with a pore size of 0.2 µm. During the research expedition, shipboard Milliq-clean water was filtered onto Sterivex (similar to Niskin bottle sampling) as field controls. Blank filters were also extracted alongside samples in the lab to represent lab-based negative controls.

During expeditions to the Gorda Ridge (includes Apollo and Seacliff vent fields) and Mid-Cayman Rise, Isobaric Gas Tight (IGT) samplers (Seewald *et al.*, 2002) were used to collect representative diffuse fluid for geochemical analyses from the same locations as samples used for molecular biology. IGT samples were processed immediately after ROV recovery. Geochemical analyses are described in Hu *et al.* (2021). Briefly, $pH_{25°C}$ was measured at room temperature in a ship-based lab using a combination Ag/AgCl reference electrode, dissolved hydrogen gas and methane were determined by gas chromatography, and 30 mL of fluid was stored to collect shore-based measurements of Mg by ion chromatography.

158 ## 2.2. Molecular sample processing & sequence analysis

159 All samples were processed identically, where RNA was extracted from approximately half of
160 each RNALater-preserved filter using a modified protocol for the Qiagen RNeasy kit (Qiagen
161 Cat No. 74104). First, the filter was separated from the RNALater and placed in a 15 mL conical
162 tube with RNase-free silica beads and 1.5 mL of lysis buffer (RLT buffer treated with **β**-
163 Mercaptoethanol), then each tube was vortexed (bead-beating) for 3 minutes. The remaining
164 RNALater was spun down for 15 minutes (14,000 rpm), supernatant removed, and 500 µl of
165 lysis buffer was added and mixed to collect any material that was previously suspended in
166 RNALater. The lysis buffers were combined and separated from the filter and silica beads before
167 continuing with the rest of the column RNA extraction, which included an in-line RNAse-free
168 DNAse removal step (Qiagen Cat No. 79256). RNA was reverse transcribed to complementary
169 DNA (Biorad Cat No. 1708841) and the V4 hypervariable region (Stoeck *et al.*, 2007) within the
170 conserved 18S rRNA gene was amplified similar to previous work (Hu *et al.*, 2021; Ollison *et*
171 *al.*, 2021). Amplified products were multiplexed, pooled at equimolar concentrations, and
172 sequenced with MiSeq 2 x 300 bp PE kit at the Marine Biological Laboratory Bay Paul Center
173 Keck sequencing facility. Amplicons from extracted RNA (amplified cDNA) were chosen for
174 this study, as they are more likely to originate from metabolically active cells, rather than
175 inactive cellular material (Blazewicz *et al.*, 2013; Hu *et al.*, 2016).
176
177 Amplicon sequences were processed together using QIIME2 v2021.4 (Bolyen *et al.*, 2019).
178 Sequences were quality controlled and primers were removed using cutadapt (error rate: 0.1,
179 minimum overlap: 3 bps)(Martin, 2011). DADA2 (Callahan *et al.*, 2016) in QIIME2 enabled
180 paired-end reads to be truncated (260 bp forward read and 225 bp reverse read), an error rate

(max-ee = 2) to be estimated, and chimeras to be identified and removed (pooled method) to ultimately determine Amplicon Sequence Variants (ASVs). DADA2 was executed on sets of sequences from the same MiSeq run and were later merged to enable comparisons across sequence runs. Resulting ASVs serve as species or strain level designations. ASVs were further clustered into "Operational Taxonomic Units" (OTUs; QIIME2, cluster vsearch *de novo*), where ASVs were grouped by percent base pair similarity at 99%, 97%, and 95%. Reference sequences for all recovered ASVs and OTUs were assigned taxonomy using vsearch (Rognes *et al.*, 2016) at 80% identity with the Protist Ribosomal database v4.14 (Guillou *et al.*, 2012; Vaulot, 2021). ASVs identified as belonging to metazoan were removed from downstream analysis, as it is outside the scope of this study. In addition to taxonomic identification, ASVs and OTUs were placed into categories based on distribution across sample types, where the 'resident' population included ASVs or OTUs that appeared only in diffuse vent fluids, and 'cosmopolitan' ASVs or OTUs were found in various sample types, and not restricted to vent fluid only. Results from OTU clustering served as a method to explore the impact that amplicon-defined species or strains may have on ecological interpretations (Supplementary Information).

2.3. Statistical analysis

ASV tables, taxonomy assignments, and sample metadata were compiled for all downstream analyses (R v4.1.0; Oksanen *et al.*, 2007; McMurdie and Holmes, 2013; Team, 2017; Wickham, 2017). Shipboard and laboratory negative control samples (MilliQ water) were compared to experimental samples to remove putative contaminant ASVs using 'decontam' (Davis *et al.*, 2018); ASVs that were 50% or more prevalent in the negative controls, relative to samples, were removed from all datasets. Amplicon sequence surveys do not necessarily equate to microbial

community biomass or metabolic activity (Blazewicz *et al.*, 2013; McMurdie and Holmes, 2014; Gloor *et al.*, 2017), and may consequently mislead interpretations of relative sequence abundance. We specifically used multiple approaches to address our questions and placed more weight on the presence and absence of protistan assemblages to interpret our results. Species richness was estimated using DivNet (Willis and Martin, 2022), which accounts for unobserved species when estimating alpha diversity, thus providing an estimate of alpha diversity variance.

Network analysis to determine putative ASV-ASV interactions (co-occurrences) was conducted using a SParse InversE Covariance Estimation for Ecological Association Inference approach (SPIEC-EASI; Kurtz *et al.*, 2015). ASVs had to appear in more than 1 sample and have at least 100 sequences to be passed through the SPIEC-EASI analysis. SPIEC-EASI glasso method was conducted with a lambda min ratio of $1e^{-2}$, nlambda = 20, and rep.num = 50. Significant ASV-ASV pairs were considered when the interaction was > |0.01|. Significantly co-occurring ASVs were evaluated by taxonomic group and ASV classification and interpreted based on the total number of occurrences and inferred functional trait of involved taxa (Ramond *et al.*, 2019).

Distance-based redundancy analysis (DBRDA; Legendre and Anderson, 1999) was performed on Euclidean distance matrices derived from center-log ratio transformed count data (Aitchison, 1986) in order to evaluate the significance of location, year, sample type, and geochemical parameters. Ahead of DBRDA, ASV count tables were subsampled to the relevant number of samples for each test (*e.g.*, across vent sites only, resident vs. cosmopolitan population, and some taxonomic groups). Code can be found at: https://shu251.github.io/microeuk-amplicon-survey/.

3. RESULTS

3.1. Fluid Composition

We examined microbial eukaryotic community composition, diversity, and distribution across four geographically distinct deep-sea hydrothermal vent fields (Figure 1). In the North East Pacific Ocean, Axial Seamount (~1520 m depth) is an active submarine volcano on the Juan de Fuca Ridge. All diffuse vent fluids from Axial Seamount are hosted in basaltic rock (Topçuoğlu *et al.*, 2016; Fortunato *et al.*, 2018), with temperatures ranging between 6.6°C and 53.2°C (Table 1). Fluids collected were slightly acidic with *in situ* pH values of 5.0-6.8 and contained up to 1 mmol/L in total dissolved hydrogen sulfide and less than 14 µmol/L dissolved hydrogen (Table 1). Samples from Marker 113 were collected over 3 years and did not reveal any clear temporal trends, with the exception of higher concentrations of bacterial and archaeal cells following the 2015 eruption (2013-2014 average: 4.0 x 10^5 cells ml^{-1}; 2015: 6.0 x 10^6 cells ml^{-1}; Table 1). Diffuse venting fluids within the Gorda Ridge ranged in temperature from 10-80°C, were slightly acidic ($pH_{25°C}$ = 5.5-6.4), and contained concentrations of dissolved hydrogen that were higher than at Axial Seamount (22-130 µmol/L; Table 1). While low-temperature diffuse venting fluid was targeted for sampling at the Mid-Cayman Rise, temperature ranges within Von Damm and Piccard were higher than in the NE Pacific, and even exceeded 100°C at Von Damm (range at Von Damm: 21-129°C and Piccard: 19-85°C). Fluids from Von Damm contained the lowest concentrations of magnesium (Table 1), indicating the fluids at this site contained a higher proportion of end-member hydrothermal vent fluid when compared to the other sites. Consistent with the influence of ultramafic rock, Von Damm vent fluids also had higher concentrations of methane and dissolved hydrogen (Table 1).

3.2. Distribution and composition of 18S rRNA gene sequences

The 18S rRNA gene tag-sequence survey across all four vent fields recovered 3.81 million sequences and 17,934 ASVs. Following corrections for contamination based on negative controls, 56 ASVs were removed, comprising 0.74% of the sequences and 0.31% of the ASVs. Samples with fewer than 20,000 sequences were also removed from the dataset (n = 2; Figure S1). The final sequence dataset used for downstream analyses includes 3.79 million sequences and 12,375 ASVs; where the mean number of sequences per sample is >88,000 (min: 25,000, max: 286,000) and ASVs per sample is 670 (min: 32, max: 2,100; Figure S1).

Protistan supergroups and phyla were detected at different relative abundances among diffusely venting fluids, plume water, and background seawater (Figures 2a and S2). Background samples were dominated by stramenopiles, dinoflagellates, and ciliates, and the plumes were largely made up of radiolaria, dinoflagellates, and ciliates. Vent fluid samples were overwhelmingly composed of ciliates, then dinoflagellates (Figures 2a and S2; Table S2). Microbial eukaryotic community composition clustered primarily by vent field, then by sample type (Jaccard dissimilarity; [0,1]; Figure 3a). Within each vent field, samples from the plume and background consistently clustered separately from diffuse vent fluid samples. Over 10,000 ASVs were unique to an individual vent field (82% of ASVs and 33% of sequences; Figures 2b, 3b, and S3). Only 194 ASVs were found in all samples (1.5% of ASVs and 22% of sequences; Figure 3b).

There were 330 ASVs shared between vent fluids from Axial Seamount and Gorda Ridge (situated ~440 km apart; Figure 2b); shared diversity between the NE Pacific vent fields included cercozoa, specifically Filosea-Sarcomonadea, *Thecofilosea*, and *Endomyxa*, and ciliates

(*Choreotrichida*, *Scuticociliates*, and *Plagiopylea*; Figure 2b). The Gorda Ridge plume sites were also characterized by the highest relative abundances of radiolaria, while the background at Gorda Ridge had comparatively fewer stramenopile and dinoflagellate sequences relative to background seawater at Axial Seamount (Figures 2a and S2).

Of the 3,586 ASVs identified from Axial Seamount, only 177 ASVs were shared across 2013, 2014, and 2015 within the vent fluid; the majority of these shared ASVs were ciliates (including members within the *Plagiopylea* and *Oligohymenophorea*; Figures 2b and S4b). While the same protistan supergroups were represented year to year at Axial Seamount, exceptions included the 2015 samples from the deep seawater and Anemone plume where the community varied with respect to the composition and the relative abundances of stramenopiles (Ochrophyta versus Opalozoa) and Rhizaria (cercozoa vs. radiolaria; Figure S2).

Despite closer proximity to one another relative to the two NE Pacific vent fields, samples from Von Damm and Piccard (~20 km apart) shared fewer ASVs (235 ASVs; Figure 2b and S3). Of these shared ASVs, a high proportion of sequences were identified as ciliates (*Plagiopylea, Spirotrichea, Strombiidia*, and *Leegaardiella*), radiolaria (Acantharia and RAD), cercozoa (Filosea-Sarcomonadea and *Bigelowiella*), and Hacrobia (Prymnesiophyceae and *Chrysochromulina*) . Shared stramenopile ASVs included MOCH (-2, -5) and MAST (-7, -4C), but typically distinct subclades were found at Von Damm and Piccard, while other stramenopile ASVs included Chrysophyceae and Dictyochophyceae.

3.3. Driving forces in microeukaryote community structure

Microbial eukaryotic communities located at greater geographic distances corresponded to more dissimilar communities (Figure 4a), while communities found at vent sites within the same vent field (<10 km apart) displayed a wide range of community dissimilarity (Figure 4a). Pairwise community comparisons for samples less than 10 km apart often showed the same level of community dissimilarity as samples situated in different ocean regions (>10,000 km; Figure 4a). Variance in community dissimilarity decreased as a factor of increasing geographic distance (Figures 4a and S5a), demonstrating a heteroscedastic relationship (triangular relationship (Cornelissen, 1999; Santini *et al.*, 2017). This observation was consistent when ASVs were subsampled to the resident and cosmopolitan populations (Figures S5b-c). Species richness, estimated by Shannon diversity via DivNet, was highest among venting fluids when compared to plume and background communities (Figure 4b). This was further supported by high ASV richness of individual protistan taxa within the vent samples (Figure S6a). Shannon diversity estimates were highest at Boca, Marker 113, and Marker 33 vent sites (Figure S6b).

ASVs were classified based on their distribution as either 'resident' (ASVs detected exclusively within diffusely venting fluid), which represented putative endemic species, or 'cosmopolitan' (ASVs found across vent, plume, and/or background sample types, Figure 3c). 65% of all ASVs were classified as resident (8,107 ASVs), while only 17.2% of the ASVs were identified as cosmopolitan (2,133 ASVs; Table S3). Further, 35% of the cosmopolitan ASVs were found within a single vent field, and only 8.7% of the cosmopolitan population was detected in all four vent fields. Within the resident ASVs, 60% (18% of all sequences) were also restricted to a single vent field (7,325 ASVs; Figures 2b, 3b-c, and S4b-d, Table S3). Only 7 ASVs were both

318 resident to diffuse venting fluid and found at every vent site; these ASVs were taxonomically
319 identified as haptophytes (*Chrysochromulina*, Prymnesiophyceae), Stramenopiles
320 (Chrysophyceae), and a choanoflagellate.
321
322 The proportion of resident versus cosmopolitan ASVs also varied by taxonomic group (Figures
323 5a and S7). Dinoflagellate, archaeplastida, and stramenopile groups had a higher proportion of
324 ASVs with a cosmopolitan distribution (Figure 5a). Within excavata, apusozoa, and amoebozoa,
325 the majority of ASVs were recovered only within diffusely venting fluid; these groups also had
326 the fewest total number of sequences assigned to them (Figure 5a). For ASVs classified as
327 resident, there was additional population heterogeneity by individual vent site (Figure 5b). For
328 instance, Euplotia (ciliates) were overrepresented in Anemone, Boca, and El Guapo in 2013 at
329 Axial Seamount and in Venti Latte at Gorda Ridge, but were found at lower relative abundances
330 at all other vent fields (Figure 5b).
331
332 Additional clustering of ASVs into OTUs at 99%, 97%, and 95% similarity resulted in consistent
333 trends in distribution, proportion of cosmopolitan vs. resident ASVs or OTUs, and the percentage
334 of resident ASVs or OTUs limited to a single vent field (Table S3). Samples situated closer
335 together were also more similar to one another when ASVs were clustered further (Figure S5d-f).
336 Overall, a similar distance-decay trend was found at 99%, 97%, and 95% sequence similarity,
337 where community dissimilarity varied at sites within the same vent field (Figure S5d-f). These
338 results demonstrate that regardless of how amplicons are determined to represent species or
339 strain taxonomic levels, the ecological interpretation of diversity across vent fluid, plume water,
340 and background seawater remains consistent.

Geochemical measurements and depth appeared to primarily influence the resident protistan population across all vent fields and regions (Figure S8). Among the individual vent sites only, the resident protistan population was found to be influenced by depth, *in situ* microbial concentration, and pH (Figure S8). The Boca vent at Axial Seamount was determined to be a significant outlier using a method to estimate homogeneity of group dispersion (O'Neill and Mathews, 2000). While some missing geochemical values compounded our ability to fully test the significance of fluid chemistry on protistan community structure, by subsampling the members of the microbial eukaryotic community based on taxonomy or distribution, some parameters were found to be significant (Figure S8; $p < 0.05$).

Network analyses were conducted to address the hypothesis that protistan nutrient strategies associated with predator-prey (phagotrophic, heterotrophic, or myzocytotic) or parasitic (host-parasite) life-styles made up the majority of significantly co-occurring ASVs (Tables 2 and S4). Ahead of Spiec Easi analysis, data was subsampled so that ASVs appeared in more than one sample and had more than or equal to 100 sequences (n = 2,575 ASVs). Putative positive and negative interactions were filtered by -0.01 and +0.01, respectively; this left over 91k putative interactions (3,363 negative and 87,925 positive, Tables 2 and S4). A higher number of putative interactions was found among ASVs detected within the same vent field (*e.g.*, ASVs from MCR to other ASVs from the region, or among Gorda Ridge-Gorda Ridge only ASVs), as well as ASVs found at all sites. Similarly, co-occurring ASVs were more likely to have positive interactions and be composed of ASVs from either the resident or cosmopolitan population (*i.e.*, a resident ASV significantly co-occurred with other resident ASVs). The most common ASV-

ASV pairs were between dinoflagellate-dinoflagellate (12% of putative interactions), ciliate-ciliate (15%), or radiolaria-dinoflagellate (5.5%). For the resident-only interactions, the majority of the ASVs were composed of ciliate-ciliate interactions, while dinoflagellate-dinoflagellate interactions made up the majority of cosmopolitan interactions.

4. DISCUSSION

Chemosynthetic bacteria and archaea are well known to form the foundation of the hydrothermal vent microbial food web (Butterfield *et al.*, 2004; Huber *et al.*, 2007; Sievert and Vetriani, 2012; McNichol *et al.*, 2018). Microbial eukaryotes serve as an important source of grazing, nutrient remineralization, and act as hosts to symbionts (Moreira, 2003; Pasulka *et al.*, 2019; Hu *et al.*, 2021). The community composition and diversity of protists has previously been studied at several deep-sea hydrothermal vents (Edgcomb *et al.*, 2002; López-García *et al.*, 2007; Murdock and Juniper, 2019). Here, we explored regional and semi-global trends in protistan diversity across multiple vent fields to gain insight into how vent geochemistry and geographic distance influence community composition and the extent of endemicity among protists. Assessments of microbial eukaryotic biodiversity and distribution in relation to vent field geochemistry is a critical part of understanding how the vent microbial food web impacts the surrounding ecosystem. We determined that individual hydrothermal vent fields display highly diverse and spatially-restricted protistan assemblages, often within individual diffuse vent sites, and that geology, vent fluid chemistry, and ocean region appear to influence microbial eukaryotic community structure. Documenting the selective processes that drive protistan communities to occupy hydrothermal vents is critical for assessing their contribution on the deep-sea microbial food web and carbon budget, which ultimately impacts the resilience of these unique ecosystems.

4.1. Protistan populations at hydrothermal vents are distinct & diverse

The warm and reduced venting fluid that rapidly mixes with the surrounding seawater creates an energy-rich habitat characterized by steep chemical and temperature gradients at diffuse vent sites. This feature makes hydrothermal vents 'biological oases' in the deep ocean, where a rich community of microorganisms, meiofauna, and macrofauna inhabit the region surrounding the vent site. When broadly classified to the supergroup and phylum level, protistan community composition was primarily composed of the alveolates, ciliates and dinoflagellates, and then Rhizaria and stramenopiles at all vent fields and sample types (diffuse fluid, plume, and background; Figures 2a and S2). Within each vent field, there was a consistent relative increase in both sequences and ASVs identified as ciliates in the vent fluid samples compared to the plume and background. Further, the protistan community composition was found to be similar to previous amplicon-based studies set at deep-sea hydrothermal vents, including the overall increase in likely heterotrophic microeukaryotes at sites of diffuse venting fluid (Edgcomb *et al.*, 2002; López-García *et al.*, 2007; Murdock and Juniper, 2019; Pasulka *et al.*, 2019; Hu *et al.*, 2021).

Regardless of oceanic region and vent field, we found microbial eukaryotic species richness to be consistently higher within diffuse venting fluids (≤100°C), compared to plume and background seawater, and have limited dispersal across samples at the strain and species-level designation (Figures 2-4 and S4, Table S3). Further, a high proportion of the protistan diversity (number of ASVs) was unique to individual vent fields, and even to single vent sites (Figures 2-4 and S4, Table S3). This observation is similar to the diversity and distribution of hydrothermal

vent bacteria and archaea, where little overlap in microbial phylotypes or strains are found at different vent sites within the same field (Huber *et al.*, 2006, 2007; Opatkiewicz *et al.*, 2009; Anderson *et al.*, 2017; Fortunato *et al.*, 2018). Varying subsurface fluid plumbing, geological features, water-rock reactions, and the metabolic activity of subsurface microorganisms cause end member vent fluid chemistries to be substantially different, even when situated only meters apart (Butterfield *et al.*, 2004; Von Damm *et al.*, 2006; McDermott *et al.*, 2018). As a result, closely-related groups of bacteria and archaea are found throughout the hydrothermal vent environment, while individual sites of diffusely venting fluid often host subpopulations that are distinct at the species level (Huber *et al.*, 2006, 2010; Opatkiewicz *et al.*, 2009). Our findings demonstrate that population heterogeneity at individual vent sites extends to microeukaryotic communities, meaning individual sites of diffusely venting fluid represent distinct populations of protistan species that exhibit 'microdiversity' relative to the broader hydrothermal vent region and surrounding deep sea.

One implication of habitat heterogeneity among protistan assemblages is that the surrounding deep-sea community may serve as a reservoir of protistan diversity, where some species exist at low abundance, but ultimately increase in abundance within the favorable conditions presented by diffuse venting fluid, such as prey or host abundances (Mars Brisbin *et al.*, 2020). This supports the idea that the hydrothermal vent environment selects for particular protistan species or their functional traits, and potentially highlights the role of the microbial rare biosphere has in community assembly (Sogin *et al.*, 2006; Caron and Countway, 2009). The existence of underexplored microbial eukaryotic biodiversity at deep-sea hydrothermal vents, including

potentially novel or endemic species, also underscores the need to document their biodiversity for conservation efforts.

4.2. Putative endemic protists restricted to individual vent fields

Deep-sea hydrothermal vents attract and host a diverse assemblage of microbial life stemming from the chemosynthetic bacteria and archaea. Microbial species found within vent fluids and largely absent from the surrounding non-hydrothermal vent environment are considered vent endemics. These putatively endemic populations are maintained over spatial and temporal scales by subsurface fluid flow and geology (Huber *et al.*, 2010). Endemicity and habitat preference among protistan species were investigated by Murdock and Juniper (2019), where network analyses revealed co-occurrences between prokaryotic extremophiles and protistan species found only at vent sites within the Mariana Arc. Findings indicated that endemicity among protists is not necessarily a general trait. Here, we add to this work by investigating functional traits that may be shared among widely-distributed vent-associated protists or potential vent endemics.

We found that over 50% of the recovered ASVs at each vent site were restricted to individual vent fluid samples only (Figure 3c), and classified as resident ASVs, or 'putative endemic' species. While resident ASVs within each vent field were dominated broadly by ciliates, resident ciliate ASVs were not typically shared across vent fields (Figures 2b and S4). Instead, ASVs classified as resident and found at all vent fields included haptophytes (*Chrysochromulina* and *Prymnesiophyceae*), stramenopiles (*Chrysophyceae*), and choanoflagellates (*Stephanocidae*). Shared traits among these protistan groups include phagotrophy and a free-living lifestyle (Caron *et al.*, 2012; Ramond *et al.*, 2019), demonstrating that phagotrophic modes of nutrition could be

455 considered a ‘general trait’ among vent-associated protists. Additionally, taxonomic groups
456 found primarily within the cosmopolitan population are also typically of mesopelagic and
457 bathypelagic protistan communities (Pernice *et al.*, 2016; Giner *et al.*, 2019).
458
459 Putative endemic taxa detected exclusively within vent fluids and largely absent from the
460 cosmopolitan population include excavata, apusozoa, and amoebozoa (Figure 5b; Table S2).
461 These groups likely represent protistan species with more specialized traits to enable vent
462 endemicity; in support of this hypothesis, these same groups were classified as rare and likely
463 endemics in Mariana Arc vent fluids (Murdock and Juniper, 2019). The taxonomic placement of
464 excavata, apusozoa, and amoebozoa is often debated, and these groups are considered candidates
465 for probing the evolutionary history and origin of unicellular eukaryotes. For instance, ASVs
466 identified as *Hicanonectes teleskopos* (excavata) are deep-branching relatives of diplomondas
467 (Park *et al.*, 2009), and excavata are widely known as a basal flagellate lineage. Species within
468 apusozoa and amoebozoa are often placed outside the eukaryotic supergroups, where apusozoa
469 have been documented as a potential sister to the Opisthokonta (Cavalier-Smith and Chao,
470 2010). A shared functional trait among excavata, apusozoa, and amoebozoa is that many species
471 are known to be amitochondriate, meaning they lack mitochondria, and instead have
472 hydrogeneosomes that are characteristic of anaerobic metabolisms (Minge *et al.*, 2009; Park *et*
473 *al.*, 2009). This suggests that a vent endemic trait among protists may include anaerobic
474 metabolism capability, thus allowing them to thrive at the interface of non-oxygenated
475 hydrothermal vent fluid and oxygenated seawater.
476

Similar to previous work, ciliates were found in all deep-sea samples, and had relatively higher abundances and high species richness within vent fluid samples (Figures 2 and 5). Ciliate trophic strategies range widely from parasitism to phagotrophy, and even symbiont hosts (Lynn, 2008), which likely explains their presence in both the cosmopolitan and resident protistan populations (Figures 2b and S7). Like the putative endemic excavata, apusozoa, and amoebozoa, some ciliate species also characteristically harbor hydrogenosomes (*e.g.*, Oligohymenophorea and Plagiopylea) (Fenchel and Finlay, 1995; Lynn, 2008; Fenchel, 2013); indicating that the oxygenated seawater interacting with diffuse venting fluid creates a favorable habitat for ciliates, similar to an oxycline (Edgcomb and Pachiadaki, 2014). While ciliates are known to have evolved the ability to thrive in sub-oxic environments multiple times, their tendency to be found along oxygen gradients is not fully understood (Rotterová *et al.*, 2022). Additionally, species of ciliates often form ecto- or endo-symbiotic relationships with bacteria or archaea. For instance, among ciliates with hydrogenosomes, methanogenic archaea have been found as endosymbionts; sulfate-reducing symbionts or methanogens benefit from intracellular hydrogen and other fermentation by-products produced by the ciliate hosts (Fenchel and Finlay, 1992; Beinart *et al.*, 2018; Rotterová *et al.*, 2022). The widespread distribution of ciliates in the deep sea, together with other accounts of deep-sea specific ciliate species signatures (Schoenle *et al.*, 2017), and observed species heterogeneity by vent site (Figure 5b), suggests that ciliate species employ a variety of more specialized feeding strategies, partnerships, and functional traits within vent-associated food webs.

4.3. Biotic & abiotic factors influence vent-associated microbial eukaryotes

Results of our study indicate that vent sites within the same region demonstrated a high degree of variability in community dissimilarly (<10 km; Figure 4a), which may be attributed to species diversity within the resident protistan population (Figures 4-5 and S5). This observed 'triangular relationship' in other ecosystems is considered a consequence of variability in abiotic factors between habitats (Cornelissen, 1999). While no single environmental parameter was found to significantly shape overall microbial eukaryotic diversity, subsampling the protistan community based on distribution (resident vs. cosmopolitan), taxonomic lineage, and vent field revealed some parameters to have an influence on protistan community composition (Figure S8). For instance, the composition of the resident protistan population found only at vent sites corresponded to depth, microbial cell concentration, and pH (Figure S8). We hypothesize that the subseafloor environment and chemistry of the diffuse fluid influences the composition of bacteria and archaea, both of which ultimately dictate protistan biomass and activity. Additional support for this hypothesis stems from previous work at the Gorda Ridge, which found evidence that protistan grazing activity may be related to microbial cell concentration (Hu *et al.*, 2021). In comparison to another route of microbial mortality at hydrothermal vents, virus biogeography at Mid-Cayman Rise and Axial Seamount were revealed to not only be spatially restricted, but to more closely correspond to microbial host distribution (Thomas *et al.*, 2021). Parameters that dictate protistan distribution and diversity at deep-sea vents likely include a combination of vent geochemistry and the composition of the vent bacterial and archaeal communities. Further, abiotic generation of organic compounds from subsurface mixing and water-rock interactions also influence microbial activity and community distribution (McDermott *et al.*, 2015, 2020).

521

522 Vent fluid geochemistry, regional geology, and subsurface fluid flow contribute to the
523 composition of the chemosynthetic bacteria and archaea at hydrothermal vents; subsequently, the
524 genetic diversity of microbial populations found in vent fluid offers insight into the fluid source
525 and subsurface environment that supports these individual microbial communities (Anderson *et*
526 *al.*, 2017; Fortunato *et al.*, 2018; Stewart *et al.*, 2019). While Von Damm and Piccard
527 hydrothermal vent fields are situated close together, protistan communities found within diffuse
528 vent fluids at each site were largely distinct (Figures 2-3, and 5). Resident ASVs identified as
529 Novel-clade 10 cercozoa were highly represented at the Piccard vent sites compared to Von
530 Damm, and inversely, ciliates belonging to the class Karyoreltica were found at higher relative
531 abundances at several vents sites at Von Damm compared to Piccard. In addition to Karyoreltica,
532 several other taxa were overrepresented at Shrimp Hole and X18, which represent the highest
533 pH, and lowest temperature vents sampled at Von Damm (Figure 5b, Table 1). Previous
534 metagenomic and metatranscriptomic analysis of Mid-Cayman Rise vent fluids revealed
535 microbial populations to be distinct and more diverse at Von Damm, relative to Piccard, while
536 the dominant metabolisms of the two communities were similar to one another (Anderson *et al.*,
537 2017). These trends were attributed to the more diverse carbon sources found at Von Damm
538 (Anderson *et al.*, 2017), emphasizing how intimately linked subseafloor processes are to the
539 genetic diversity of vent-associated microbial communities.

540

541 ### 4.4. Presumed trophic strategy among vent-associated protists

542 Microbial eukaryotes contribute to the hydrothermal vent food web as consumers of
543 chemosynthetic microorganisms or other microbes, and therefore directly impact carbon flux to

544 the surrounding environment. Taxon-specific differences in the composition of resident and
545 cosmopolitan protistan populations provide some evidence that species distribution is also linked
546 to protistan physiology. The cosmopolitan protistan population had a similar taxonomic
547 breakdown to studies situated in mesopelagic to bathypelagic depths; the protistan communities
548 at these depths are often dominated by cercozoa, Rhizaria, and stramenopiles, especially MArine
549 STramenopiles (MAST clades) (Figure 2b; Pernice *et al.*, 2015, 2016; Giner *et al.*, 2019).
550 Members of the Rhizaria and stramenopiles are well known to inhabit every depth in the water
551 column and are typically heterotrophic. This suggests that a shared generalist trait among widely
552 distributed deep-sea protists that also thrive at hydrothermal vents may include phagotrophy.
553
554 In an effort to explore the relationships between putative trophic mode and species distribution,
555 we highlight the prevalence of predator-prey and parasite-host interactions. We targeted ASVs
556 co-occurring at significant levels (derived from network analyses) that are also hypothesized to
557 include known predators or parasites (Ramond *et al.*, 2019) (Table 2; Table S4). Many of the co-
558 occurring ASVs were derived from the same lineage, indicating that we cannot exclude the
559 possibility that the interactions reflect species responding to similar environmental parameters.
560 Phagotrophy was a prominent nutritional strategy shared among the most frequently co-
561 occurring ASVs (Table 2), and likely includes a range of phagotrophic feeding strategies. For
562 instance, dinoflagellate and ciliate phagotrophs are known to actively target and hunt preferred
563 prey; including the use of raptorial feeding (consumption of prey larger than the predator), the
564 use of chemical cues to detect prey, or employing a 'feeding current' to intercept and capture
565 prey (Fenchel, 1980; Verity, 1991; Table 3; Pernthaler, 2005; Leander, 2020). The other main
566 trophic strategies identified included parasitism or myzocytosis (Guillou *et al.*, 2008; Leander,

2020) specifically within cercozoa, Syndiniales, and some ciliates (Table 2). Parasitism likely plays an important, yet understudied role, in hydrothermal vent food webs, and hosts of protistan parasites include other protists, fishes, or even multicellular metazoa (Moreira, 2003; Govenar, 2012). Broadly, the frequency of putative predator-prey and host-parasite interactions suggests that diffuse venting fluids provide an oasis of increased prey and host availability for the deep-sea protistan population. Additionally, the prevalence of protistan parasites demonstrates a potential linkage between microbial and macrofaunal trophic levels at submarine hydrothermal vents.

4.5. Summary & Broader implications

Hydrothermal vent fields from the NE Pacific and the western Caribbean were composed of a mixture of globally-distributed and regionally-specific protistan species. While most major lineages of protists were detected across the diffuse venting fluid, plume, and deep seawater samples, populations at the species level were distinct to a single vent field or even to an individual vent site within a field. Additionally, no single parameter explained protistan community structure across the vent, plume, and background environment; instead, only the protistan community restricted to diffuse venting fluid appeared to be influenced by depth, cell concentration, and pH.

Deep-sea hydrothermal vents are oases of microbial diversity that sustain chemosynthetic-fueled deep-sea food webs. By characterizing the taxonomic composition and distribution of protistan communities across geographically-separated vent fields we highlight some of the mechanisms that may lead to selection, and likely speciation, of microbial eukaryotes at hydrothermal vents.

Understanding these sources of speciation and how protistan biodiversity is linked to the hydrothermal vent ecosystem are critical for understanding how disruptive events may harm these habitats (Orcutt *et al.*, 2020). Investigating shared trophic strategies of vent-associated versus cosmopolitan protistan species also demonstrates how species distribution may influence food web interactions and the composition of microbial prey. Deep-sea hydrothermal vents are vulnerable to disruptive events that cause interruptions in vent food web mechanisms (Van Audenhaege *et al.*, 2019). Thus, studies that emphasize global to local biodiversity dynamics can be used to evaluate ecosystem health and provide important context for modeling food web dynamics that consider different trophic strategies.

Data Availability

Raw sequence data are available through NCBI. SRA BioProject accession numbers are PRJNA637089 for Gorda Ridge, PRJNA641911 for Axial Seamount, and PRJNA802868 for Mid-Cayman Rise. Sequences, QIIME2 artifact files, and other data are available at Zenodo: 10.5281/zenodo.5959694. Processed ASV count files, taxonomy assignments, and code to reproduce results, regenerate figures, and perform statistical tests are available at: https://shu251.github.io/microeuk-amplicon-survey/.

ACKNOWLEDGEMENTS

We would like to thank everyone involved in the collection and processing of diffuse vent fluid, including Nicole Raineault, Margrethe Serres, Karyn Rogers, Tom McCollom, and the captains and crews of the EV Nautilus, RV Falkor, RV Thompson, RV Brown, as well as the pilots and engineers for ROV ROPOS, ROV Jason, and ROV Hercules. Authors would also like to acknowledge helpful discussion and contributions from Olivia Ahren and Margaret Mars Brisbin. Work conducted at Axial Seamount was supported by the Gordon and Betty Moore Foundation (Grant GBMF3297 to J.A.H), Schmidt Ocean Institute, National Oceanic and Atmospheric Administration (NOAA) Pacific Marine Environmental Lab (contribution number 5407), the Joint Institute for Study of the Atmosphere and Oceans (NOAA Cooperative Agreement NA15OAR4320063) contribution number 2022-1219, and the Cooperative Institution for Climate, Ocean, and Ecosystem Studies (CICOES) contribution number 2022-1219. Research from the Gorda Ridge was supported by the Ocean Exploration Trust's *Nautilus* Exploration Program, Cruise NA-108, NASA Planetary Science and Technology Through Analog Research (PSTAR) Program (NNH16ZDA001N-PSTAR) grant (16-PSTAR16_2-0011) to D.L., NASA grant (80NSSC19K1427) to C.R.G. NOAA Office of Ocean Exploration and Research Grant NA17OAR0110336, and NSF Ocean Technology & Interdisciplinary Coordination (OCE-1636510 to J.A.B.). This is SUBSEA contribution number SUBSEA-2022-001. Funding support for the Mid-Cayman Rise expedition was provided by NSF-OCE 1801036 (to S.Q.L), 1801205 to (J.S.S), NSF-OCE 1816652, and NASA Planetary Science and Technology Through Analog Research (PSTAR) Program 80NSSC17K0252 (K.F. and S.Q.L.). Support for sample processing and data analysis was also provided by the Charles E. Hollister Endowed Fund for Support of Innovative Research at Woods Hole Oceanographic Institution (WHOI). The NSF Center for Dark Energy Biosphere Investigations (C-DEBI) supported J.A.H. as well as S.K.H. through a C-DEBI Postdoctoral Fellowship (OCE-0939564). Research and analysis were also supported through an NSF grant (OCE-1947776) awarded to J.A.H. This is C-DEBI contribution number 600.

REFERENCES

Aitchison, J. (1986) The Statistical Analysis of Compositional Data.

Akerman, N.H., Butterfield, D.A., and Huber, J.A. (2013) Phylogenetic diversity and functional gene patterns of sulfur-oxidizing subseafloor Epsilonproteobacteria in diffuse hydrothermal vent fluids. *Front Microbiol* **4**:.

Anderson, R.E., Reveillaud, J., Reddington, E., Delmont, T.O., Eren, A.M., McDermott, J.M., et al. (2017) Genomic variation in microbial populations inhabiting the marine subseafloor at deep-sea hydrothermal vents. *Nat Commun* **8**:.

Atkins, M., Anderson, O., and Wirsen, C. (1998) Effect of hydrostatic pressure on the growth rates and encystment of flagellated protozoa isolated from a deep-sea hydrothermal vent and a deep shelf region. *Mar Ecol Prog Ser* **171**: 85–95.

Atkins, M.S., Teske, A.P., and Anderson, O.R. (2000) A Survey of Flagellate Diversity at Four Deep-Sea Hydrothermal Vents in the Eastern Pacific Ocean Using Structural and Molecular Approaches. *J Eukaryot Microbiol* **47**: 400–411.

Baker, E.T., Walker, S.L., Chadwick, W.W., Jr, Butterfield, D.A., Buck, N.J., and Resing, J.A. (2019) Posteruption enhancement of hydrothermal activity: A 33-year, multieruption time series at axial seamount (Juan de fuca ridge). *Geochem Geophys Geosyst* **20**: 814–828.

Baumgartner, M., Stetter, K.O., and Foissner, W. (2002) Morphological, Small Subunit rRNA, and Physiological Characterization of Trimyema minutum (Kahl, 1931), an Anaerobic Ciliate from Submarine Hydrothermal Vents Growing from 28oC to 52oC. *J Eukaryot Microbiol* **49**: 227–238.

Beinart, R.A., Rotterová, J., Čepička, I., Gast, R.J., and Edgcomb, V.P. (2018) The genome of an endosymbiotic methanogen is very similar to those of its free-living relatives: Genome of an intracellular archaeum. *Environ Microbiol* **20**: 2538–2551.

Bell, J.B., Woulds, C., and van Oevelen, D. (2017) Hydrothermal activity, functional diversity and chemoautotrophy are major drivers of seafloor carbon cycling. *Sci Rep* **7**: 12025.

Bennett, S.A., Coleman, M., Huber, J.A., Reddington, E., Kinsey, J.C., McIntyre, C., et al. (2013) Trophic regions of a hydrothermal plume dispersing away from an ultramafic-hosted vent-system: Von Damm vent-site, Mid-Cayman Rise. *Geochem Geophys Geosyst* **14**: 317–327.

712 Biard, T. (2022) Diversity and ecology of Radiolaria in modern oceans. *Environ Microbiol* **24**:
713 2179–2200.
714 Blazewicz, S.J., Barnard, R.L., Daly, R.A., and Firestone, M.K. (2013) Evaluating rRNA as an
715 indicator of microbial activity in environmental communities: limitations and uses. *ISME*
716 *J* **7**: 2061–2068.
717 Bolyen, E., Rideout, J.R., Dillon, M.R., Bokulich, N.A., Abnet, C.C., Al-Ghalith, G.A., et al.
718 (2019) Reproducible, interactive, scalable and extensible microbiome data science using
719 QIIME 2. *Nat Biotechnol* **37**: 852–857.
720 Breier, J.A., Sheik, C.S., Gomez-Ibanez, D., Sayre-McCord, R.T., Sanger, R., Rauch, C., et al.
721 (2014) A large volume particulate and water multi-sampler with in situ preservation for
722 microbial and biogeochemical studies. *Deep Sea Res Part I* **94**: 195–206.
723 Butterfield, D.A., Roe, K.K., Lilley, M.D., Huber, J.A., Baross, J.A., Embley, R.W., and
724 Massoth, G.J. (2004) Mixing, reaction and microbial activity in the sub-seafloor revealed
725 by temporal and spatial variation in diffuse flow vents at Axial Volcano. *The Subseafloor*
726 *Biosphere at Mid-Ocean Ridges* **144**: 269–289.
727 Callahan, B.J., McMurdie, P.J., Rosen, M.J., Han, A.W., Johnson, A.J.A., and Holmes, S.P.
728 (2016) DADA2: High-resolution sample inference from Illumina amplicon data. *Nat*
729 *Methods* **13**: 581–583.
730 Canals, O., Obiol, A., Muhovic, I., Vaqué, D., and Massana, R. (2020) Ciliate diversity and
731 distribution across horizontal and vertical scales in the open ocean. *Mol Ecol* **29**: 2824–
732 2839.
733 Caron, D. and Countway, P. (2009) Hypotheses on the role of the protistan rare biosphere in a
734 changing world. *Aquat Microb Ecol* **57**: 227–238.
735 Caron, D.A., Countway, P.D., Jones, A.C., Kim, D.Y., and Schnetzer, A. (2012) Marine
736 Protistan Diversity. *Ann Rev Mar Sci* **4**: 467–493.
737 Cavalier-Smith, T. and Chao, E.E. (2010) Phylogeny and evolution of apusomonadida (protozoa:
738 apusozoa): new genera and species. *Protist* **161**: 549–576.
739 Cornelissen, J.H.C. (1999) A triangular relationship between leaf size and seed size among
740 woody species: allometry, ontogeny, ecology and taxonomy. *Oecologia* **118**: 248–255.
741 Davis, N.M., Proctor, D.M., Holmes, S.P., Relman, D.A., and Callahan, B.J. (2018) Simple
742 statistical identification and removal of contaminant sequences in marker-gene and
743 metagenomics data. *Microbiome* **6**: 226.
744 Edgcomb, V.P., Kysela, D.T., Teske, A., Gomez, A. de V., and Sogin, M.L. (2002) Benthic
745 Eukaryotic Diversity in the Guaymas Basin Hydrothermal Vent Environment. *Proc Natl*
746 *Acad Sci U S A* **99**: 7658–7662.
747 Edgcomb, V.P. and Pachiadaki, M. (2014) Ciliates along Oxyclines of Permanently Stratified
748 Marine Water Columns. *J Eukaryot Microbiol* **61**: 434–445.
749 Fenchel, T. (2013) Ecology of Protozoa: The Biology of Free-living Phagotropic Protists,
750 Springer-Verlag.
751 Fenchel, T. (1980) Suspension feeding in ciliated protozoa: Functional response and particle size
752 selection. *Microb Ecol* **6**: 1–11.
753 Fenchel, T. and Finlay, B.J. (1995) Ecology and evolution in anoxic worlds.
754 Fenchel, T. and Finlay, B.J. (1992) Production of methane and hydrogen by anaerobic ciliates
755 containing symbiotic methanogens. *Arch Microbiol* **157**: 475–480.
756 Fortunato, C.S., Larson, B., Butterfield, D.A., and Huber, J.A. (2018) Spatially distinct,
757 temporally stable microbial populations mediate biogeochemical cycling at and below the

seafloor in hydrothermal vent fluids: Microbial genomics at axial seamount. *Environ Microbiol* **20**: 769–784.

Giner, C.R., Pernice, M.C., Balagué, V., Duarte, C.M., Gasol, J.M., Logares, R., and Massana, R. (2019) Marked changes in diversity and relative activity of picoeukaryotes with depth in the world ocean. *ISME J.*

Gloor, G.B., Macklaim, J.M., Pawlowsky-Glahn, V., and Egozcue, J.J. (2017) Microbiome Datasets Are Compositional: And This Is Not Optional. *Front Microbiol* **8**:.

Govenar, B. (2012) Energy transfer through food webs at hydrothermal vents: Linking the lithosphere to the biosphere. *Oceanography* **25**: 246–255.

Guillou, L., Bachar, D., Audic, S., Bass, D., Berney, C., Bittner, L., et al. (2012) The Protist Ribosomal Reference database (PR2): a catalog of unicellular eukaryote Small Sub-Unit rRNA sequences with curated taxonomy. *Nucleic Acids Res* **41**: D597–D604.

Guillou, L., Viprey, M., Chambouvet, A., Welsh, R.M., Kirkham, A.R., Massana, R., et al. (2008) Widespread occurrence and genetic diversity of marine parasitoids belonging to *Syndiniales* (*Alveolata*). *Environ Microbiol* **10**: 3349–3365.

Hess, S. and Suthaus, A. (2022) The Vampyrellid Amoebae (Vampyrellida, Rhizaria). *Protist* **173**: 125854.

Hu, S.K., Campbell, V., Connell, P., Gellene, A.G., Liu, Z., Terrado, R., and Caron, D.A. (2016) Protistan diversity and activity inferred from RNA and DNA at a coastal ocean site in the eastern North Pacific. *FEMS Microbiol Ecol* fiw050.

Hu, S.K., Herrera, E.L., Smith, A.R., Pachiadaki, M.G., Edgcomb, V.P., Sylva, S.P., et al. (2021) Protistan grazing impacts microbial communities and carbon cycling at deep-sea hydrothermal vents. *Proc Natl Acad Sci U S A* **118**:.

Huber, J.A., Butterfield, D.A., and Baross, J.A. (2006) Diversity and distribution of subseafloor Thermococcales populations in diffuse hydrothermal vents at an active deep-sea volcano in the northeast Pacific Ocean: DIVERSITY OF SUBSEAFLOOR THERMOCOCCALES. *Journal of Geophysical Research: Biogeosciences* **111**:.

Huber, J.A., Cantin, H.V., Huse, S.M., Welch, D.B.M., Sogin, M.L., and Butterfield, D.A. (2010) Isolated communities of Epsilonproteobacteria in hydrothermal vent fluids of the Mariana Arc seamounts. *FEMS Microbiol Ecol* **73**: 538–549.

Huber, J.A., Mark Welch, D.B., Morrison, H.G., Huse, S.M., Neal, P.R., Butterfield, D.A., and Sogin, M.L. (2007) Microbial Population Structures in the Deep Marine Biosphere. *Science* **318**: 97–100.

Kurtz, Z.D., Müller, C.L., Miraldi, E.R., Littman, D.R., Blaser, M.J., and Bonneau, R.A. (2015) Sparse and compositionally robust inference of microbial ecological networks. *PLoS Comput Biol* **11**: e1004226.

Lang, S.Q. and Benitez-Nelson, B. (2021) Hydrothermal Organic Geochemistry (HOG) sampler for deployment on deep-sea submersibles. *Deep Sea Res Part I* **173**: 103529.

Leander, B.S. (2020) Predatory protists. *Curr Biol* **30**: R510–R516.

Legendre, P. and Anderson, M.J. (1999) DISTANCE-BASED REDUNDANCY ANALYSIS: TESTING MULTISPECIES RESPONSES IN MULTIFACTORIAL ECOLOGICAL EXPERIMENTS. *Ecological Monographs* **69**: 1–24.

Lima-Mendez, G., Faust, K., Henry, N., Decelle, J., Colin, S., Carcillo, F., et al. (2015) Determinants of community structure in the global plankton interactome. *Science* **348**: 1262073–1262073.

López-García, P., Philippe, H., Gail, F., and Moreira, D. (2003) Autochthonous eukaryotic

804 diversity in hydrothermal sediment and experimental microcolonizers at the Mid-Atlantic
805 Ridge. *Proc Natl Acad Sci U S A* **100**: 697–702.
806 López-García, P., Vereshchaka, A., and Moreira, D. (2007) Eukaryotic diversity associated with
807 carbonates and fluid?seawater interface in Lost City hydrothermal field. *Environ*
808 *Microbiol* **9**: 546–554.
809 Lynn, D. (2008) The Ciliated Protozoa: Characterization, Classification, and Guide to the
810 Literature, Springer Science & Business Media.
811 Mars Brisbin, M., Conover, A.E., and Mitarai, S. (2020) Influence of Regional Oceanography
812 and Hydrothermal Activity on Protist Diversity and Community Structure in the Okinawa
813 Trough. *Microb Ecol*.
814 Martin, M. (2011) Cutadapt removes adapter sequences from high-throughput sequencing reads.
815 *EMBnet.journal* **17**: 10–12.
816 McDermott, J.M., Seewald, J.S., German, C.R., and Sylva, S.P. (2015) Pathways for abiotic
817 organic synthesis at submarine hydrothermal fields. *Proc Natl Acad Sci U S A* **112**: 7668–
818 7672.
819 McDermott, J.M., Sylva, S.P., Ono, S., German, C.R., and Seewald, J.S. (2020) Abiotic redox
820 reactions in hydrothermal mixing zones: Decreased energy availability for the subsurface
821 biosphere. *Proc Natl Acad Sci U S A* **117**: 20453–20461.
822 McDermott, J.M., Sylva, S.P., Ono, S., German, C.R., and Seewald, J.S. (2018) Geochemistry of
823 fluids from Earth's deepest ridge-crest hot-springs: Piccard hydrothermal field, Mid-
824 Cayman Rise. *Geochim Cosmochim Acta* **228**: 95–118.
825 McMurdie, P.J. and Holmes, S. (2013) phyloseq: an R package for reproducible interactive
826 analysis and graphics of microbiome census data. *PLoS One* **8**: e61217.
827 McMurdie, P.J. and Holmes, S. (2014) Waste Not, Want Not: Why Rarefying Microbiome Data
828 Is Inadmissible. *PLoS Comput Biol* **10**: e1003531.
829 McNichol, J., Stryhanyuk, H., Sylva, S.P., Thomas, F., Musat, N., Seewald, J.S., and Sievert,
830 S.M. (2018) Primary productivity below the seafloor at deep-sea hot springs. *Proceedings*
831 *of the National Academy of Sciences* **115**: 6756–6761.
832 Minge, M.A., Silberman, J.D., Orr, R.J.S., Cavalier-Smith, T., Shalchian-Tabrizi, K., Burki, F.,
833 et al. (2009) Evolutionary position of breviate amoebae and the primary eukaryote
834 divergence. *Proceedings of the Royal Society B: Biological Sciences* **276**: 597–604.
835 Moreira, D. (2003) Are hydrothermal vents oases for parasitic protists? *Trends Parasitol* **19**:
836 556–558.
837 Murdock, S.A. and Juniper, S.K. (2019) Hydrothermal vent protistan distribution along the
838 Mariana arc suggests vent endemics may be rare and novel. *Environ Microbiol* **21**: 3796–
839 3815.
840 Oksanen, J., Kindt, R., Legendre, P., O'Hara, B., Stevens, M.H.H., Oksanen, M.J., and Suggests,
841 M. (2007) The vegan package. *Community ecology package* **10**: 719.
842 Ollison, G.A., Hu, S.K., Mesrop, L.Y., DeLong, E.F., and Caron, D.A. (2021) Come rain or
843 shine: Depth not season shapes the active protistan community at station ALOHA in the
844 North Pacific Subtropical Gyre. *Deep Sea Res Part 1 Oceanogr Res Pap* **170**: 103494.
845 O'Neill, M.E. and Mathews, K. (2000) A Weighted Least Squares Approach to Levene's Test of
846 Homogeneity of Variance. *Australian New Zealand Journal of Statistics* **42**: 81–100.
847 Opatkiewicz, A.D., Butterfield, D.A., and Baross, J.A. (2009) Individual hydrothermal vents at
848 Axial Seamount harbor distinct subseafloor microbial communities. *FEMS Microbiol*
849 *Ecol* **70**: 413–424.

Orcutt, B.N., Bradley, J.A., Brazelton, W.J., Estes, E.R., Goordial, J.M., Huber, J.A., et al. (2020) Impacts of deep-sea mining on microbial ecosystem services. *Limnol Oceanogr* **65**: 1489–1510.

Park, J.S., Kolisko, M., Heiss, A.A., and Simpson, A.G.B. (2009) Light microscopic observations, ultrastructure, and molecular phylogeny of Hicanonectes teleskopos n. g., n. sp., a deep-branching relative of diplomonads. *J Eukaryot Microbiol* **56**: 373–384.

Pasulka, A., Hu, S.K., Countway, P.D., Coyne, K.J., Cary, S.C., Heidelberg, K.B., and Caron, D.A. (2019) SSU rRNA Gene Sequencing Survey of Benthic Microbial Eukaryotes from Guaymas Basin Hydrothermal Vent. *J Eukaryot Microbiol* jeu.12711.

Pernice, M.C., Forn, I., Gomes, A., Lara, E., Alonso-Sáez, L., Arrieta, J.M., et al. (2015) Global abundance of planktonic heterotrophic protists in the deep ocean. *ISME J* **9**: 782–792.

Pernice, M.C., Giner, C.R., Logares, R., Perera-Bel, J., Acinas, S.G., Duarte, C.M., et al. (2016) Large variability of bathypelagic microbial eukaryotic communities across the world's oceans. *ISME J* **10**: 945–958.

Pernthaler, J. (2005) Predation on prokaryotes in the water column and its ecological implications. *Nat Rev Microbiol* **3**: 537–546.

Ramond, P., Sourisseau, M., Simon, N., Romac, S., Schmitt, S., Rigaut-Jalabert, F., et al. (2019) Coupling between taxonomic and functional diversity in protistan coastal communities: Functional diversity of marine protists. *Environ Microbiol* **21**: 730–749.

Rognes, T., Flouri, T., Nichols, B., Quince, C., and Mahé, F. (2016) VSEARCH: a versatile open source tool for metagenomics. *PeerJ* **4**: e2584.

Rotterová, J., Edgcomb, V.P., Čepička, I., and Beinart, R. (2022) Anaerobic ciliates as a model group for studying symbioses in oxygen-depleted environments. *J Eukaryot Microbiol* e12912.

Ryan, W.B.F., Carbotte, S.M., Coplan, J., O'Hara, S., Melkonian, A., Arko, R., et al. (2009) Global Multi-Resolution Topography (GMRT) synthesis data set. G-cubed 10 (3), Q03014.

Santini, B.A., Hodgson, J.G., Thompson, K., Wilson, P.J., Band, S.R., Jones, G., et al. (2017) The triangular seed mass–leaf area relationship holds for annual plants and is determined by habitat productivity. *Funct Ecol* **31**: 1770–1779.

Sauvadet, A.-L., Gobet, A., and Guillou, L. (2010) Comparative analysis between protist communities from the deep-sea pelagic ecosystem and specific deep hydrothermal habitats: Protist associated with hydrothermal environments. *Environ Microbiol* **12**: 2946–2964.

Schoenle, A., Hohlfeld, M., Rosse, M., Filz, P., Wylezich, C., Nitsche, F., and Arndt, H. (2020) Global comparison of bicosoecid Cafeteria-like flagellates from the deep ocean and surface waters, with reorganization of the family Cafeteriaceae. *Eur J Protistol* **73**: 125665.

Schoenle, A., Nitsche, F., Werner, J., and Arndt, H. (2017) Deep-sea ciliates: Recorded diversity and experimental studies on pressure tolerance. *Deep Sea Res Part I* **128**: 55–66.

Seewald, J.S., Doherty, K.W., Hammar, T.R., and Liberatore, S.P. (2002) A new gas-tight isobaric sampler for hydrothermal fluids. *Deep Sea Res Part I* **49**: 189–196.

Sievert, S.M. and Vetriani, C. (2012) Chemoautotrophy at deep-sea vents: past, present, and future. *Oceanography* **25**: 218–233.

Small, E.B. and Gross, M.E. (1985) Preliminary observations of protistan organisms, especially ciliates, from the 21 N hydrothermal vent site. *Bull Biol Soc Wash* 401–410.

Sogin, M.L., Morrison, H.G., Huber, J.A., Welch, D.M., Huse, S.M., Neal, P.R., et al. (2006) Microbial diversity in the deep sea and the underexplored "'rare biosphere."' *Proceedings of the National Academy of Sciences* **103**: 6.

Spietz, R.L., Butterfield, D.A., Buck, N.J., Larson, B.I., Chadwick, W.W., Walker, S.L., et al. (2018) Deep-Sea Volcanic Eruptions Create Unique Chemical and Biological Linkages Between the Subsurface Lithosphere and the Oceanic Hydrosphere. *Oceanography* **31**: 128–135.

Stewart, L.C., Algar, C.K., Fortunato, C.S., Larson, B.I., Vallino, J.J., Huber, J.A., et al. (2019) Fluid geochemistry, local hydrology, and metabolic activity define methanogen community size and composition in deep-sea hydrothermal vents. *ISME J* **13**: 1711–1721.

Stoeck, T., Zuendorf, A., Breiner, H.-W., and Behnke, A. (2007) A Molecular Approach to Identify Active Microbes in Environmental Eukaryote Clone Libraries. *Microb Ecol* **53**: 328–339.

Team, R.C. (2017) R: A language and environment for statistical com-puting.

Thomas, E., Anderson, R.E., Li, V., Rogan, L.J., and Huber, J.A. (2021) Diverse Viruses in Deep-Sea Hydrothermal Vent Fluids Have Restricted Dispersal across Ocean Basins. *mSystems* **6**: e0006821.

Topçuoğlu, B.D., Stewart, L.C., Morrison, H.G., Butterfield, D.A., Huber, J.A., and Holden, J.F. (2016) Hydrogen Limitation and Syntrophic Growth among Natural Assemblages of Thermophilic Methanogens at Deep-sea Hydrothermal Vents. *Front Microbiol* **7**: 1240.

Van Audenhaege, L., Fariñas-Bermejo, A., Schultz, T., and Lee Van Dover, C. (2019) An environmental baseline for food webs at deep-sea hydrothermal vents in Manus Basin (Papua New Guinea). *Deep Sea Res Part I* **148**: 88–99.

Vaulot, D. (2021) pr2database/pr2database: PR2 version 4.14.0.

Verity, P.G. (1991) Feeding in planktonic protozoans: evidence for non-random acquisition of prey. *J Protozool* **38**: 69–76.

Von Damm, K.L., Parker, C.M., Lilley, M.D., Clague, D.A., Zierenberg, R.A., Olson, E.J., and McClain, J.S. (2006) Chemistry of vent fluids and its implications for subsurface conditions at Sea Cliff hydrothermal field, Gorda Ridge: CHEMISTRY OF VENT FLUIDS. *Geochem Geophys Geosyst* **7**:.

Wickham, H. (2017) The tidyverse. *R package ver* **1**: 1.

Willis, A.D. and Martin, B.D. (2022) Estimating diversity in networked ecological communities. *Biostatistics* **23**: 207–222.

Živaljić, S., Schoenle, A., Scherwass, A., Hohlfeld, M., Nitsche, F., and Arndt, H. (2020) Influence of hydrostatic pressure on the behaviour of three ciliate species isolated from the deep-sea floor. *Mar Biol* **167**: 63.

[*dataset*] Hu, Sarah, & Huber, Julie. (2022). Diversity & distribution of microeukaryotes at deep-sea hydrothermal vents. https://doi.org/10.5281/zenodo.5959694

[*dataset*] Hu, Sarah (2022). Diversity & distribution of microeukaryotes at deep-sea hydrothermal vents. https://github.com/shu251/microeuk-amplicon-survey

Data Accessibility Statement

Raw sequence data are available through SRA BioProjects: PRJNA637089 for Gorda Ridge, PRJNA641911 for Axial Seamount, and PRJNA802868 for Mid-Cayman Rise. Data files can be downloaded from Zenodo: 10.5281/zenodo.5959694. GitHub repo includes all relevant code and input data, https://github.com/shu251/microeuk-amplicon-survey. All code to reproduce analyses can be found at a hosted website https://shu251.github.io/microeuk-amplicon-survey/.

Benefit-Sharing Statement

Benefits from this research culminate from the sharing of our data, results, and code necessary to reproduce results.

FIGURE & TABLE LEGENDS

Figure 1. Map of all vent fields, where symbols represent each vent site at Axial Seamount (a), (b) the two regions sampled at the Gorda Ridge, and (c) the Piccard and Von Damm vent fields along the Mid-Cayman Rise. Figure made with GeoMapApp (www.geomapapp.org) / CC BY / CC BY (Ryan *et al.*, 2009).

Figure 2. (**a**) Proportion of sequences belonging to main protistan supergroup and phyla, by sample type (left to right: Background, Plume, and Vent) and hydrothermal vent field (top to bottom: Axial Seamount, Gorda Ridge, Piccard, and Von Damm. ASVs with fewer than 200 sequences were removed. (**b**) Total number of shared (or unique) ASVs across sample type and vent field. Dot matrix below the bar plot indicates the samples included in the bar plot representation, where the bar plots above a single dot indicate that those ASVs were restricted to that vent field and sample type. Colors represent main protistan taxonomic groups. Dashed line indicates 200 ASVs were shared (y-axis); Figure S3 includes a comparison of samples with $\leq$200 ASVs.

Figure 3. (**a**) Community diversity clustered by Jaccard Dissimilarity, where values closer to 0 indicate samples are identical. (**b**) Proportion of ASVs shown by distribution among hydrothermal vent sites, Axial, Gorda Ridge, Piccard, and Von Damm (where Mid-Cayman Rise is abbreviated MCR and includes Piccard and/or Von Damm). (**c**) Proportion of ASVs designated as vent only (resident or putative endemic), cosmopolitan (found among background, plume, and diffuse vent fluid), plume only, or background only.

Figure 4. (**a**) Distance-decay plot, where data points represent pairwise comparisons of all samples (Distance-decay with resident and cosmopolitan populations can be found in Figure S4), and distance between the samples is represented on the x-axis with the community dissimilarity (estimated by Jaccard) is represented along the y-axis. Comparison of Jaccard distance variance to geographic distance is also reported in Figure S4. Note that geographic distances represent the calculated difference between latitude and longitude (Table 1), rather than oceanographic distances. (**b**) Violin plot of estimated Shannon values (derived from DivNet), by sample type (x-axis), background, plume, and vent site.

Figure 5. (**a**) Relative proportion of ASVs classified as resident (y-axis) versus cosmopolitan (x-axis). Bubble size is equivalent to the total number of sequences and color represents each supergroup. (**b**) Vent-only (putative endemic) taxa represented by CLR transformed data (red to blue) by vent sample (x-axis) and taxonomic class (y-axis). Sum of CLR transformed data will equal 0, where the log of the ratio between each data point at the geometric mean of the dataset is calculated.

Figure S1. (**a**) Total number of ASVs and (**b**) sequences in each sample of the sequence survey. Samples with fewer than 20,000 sequences were removed from the dataset.

Figure S2. Relative sequence abundance for all major protistan taxonomic groups. Colors denote

taxonomic group assignment, bar plots are organized by vent field, year sampled, and sample type.

Figure S3. Supplement to Figure 2b showing a higher resolution view of the total number of shared (or unique) ASVs across sample types that totaled to ≤200 ASVs. Dot matrix below the bar plot indicates the samples included in the bar plot representation, where the bar plots above a single dot indicate that ASVs were restricted to that single vent field and sample type. Colors represent main protistan taxonomic groups.

Figure S4. Total number of shared (or unique) ASVs at the genus level (**a**) or at the ASV level (**b-d**) for each vent field. Dot matrix below the bar plot indicates the samples included in the bar plot representation, where the bar plots above a single dot indicate that genera or ASVs were restricted to that single vent field and sample type. Colors represent main protistan taxonomic groups. Panels represent (**a**) ASVs grouped to the Genus level to show homology across vent fields, (**b**) ASVs at all the Axial Seamount samples, (**c**) ASVs at the Gorda Ridge, and (**d**) ASVs at the Mid-Cayman Rise.

Figure S5. (**a**) Variance in Jaccard dissimilarity by vent field and sample types (y-axis) relative to geographic distance (x-axis). Distance-decay plots with Jaccard Dissimilarity (y-axis) and distance (km; x-axis) for the (**b**) resident population and (**c**) cosmopolitan populations. (**d-f**) Analysis was repeated following further clustering of the ASVs into OTUs at 95%, 97%, and 99% sequence similarity. Figure 4 in the main text includes all samples and ASVs in the sequence survey.

Figure S6. (**a**) ASV richness by individual taxonomic group. Each panel represents a taxonomic group, and is denoted by color. From left to right, each panel includes a box plot representation of the ASV richness by sample type: background, plume, and vent. (**b**) Estimated Shannon values with variance (y-axis with error bars) derived from DivNet (Willis and Martin, 2022), for each sample (x-axis).

Figure S7. Distribution of cosmopolitan versus resident (**a**) sequences and (**b**) total ASVs by taxonomic group (color) and vent field (x-axis).

Figure S8. Results from distance-based redundancy analysis (DBRDA) to determine if environmental factors (top, x-axis; *i.e.*, fluid chemistry, temperature, and microbial cell counts) play a significant role in shaping community dissimilarity. Analysis was conducted on subsets of the samples collected (panels from left to right) and of the ASVs recovered (rows, y-axis). By subsampling the data ahead of DBRDA, we were able to focus on different components of the deep-sea microbial eukaryotic community (*e.g.,* the resident population, NE Pacific Ocean vent fields only, or only Mid-Cayman Rise). All geochemical values used are also reported in Table 1. Color designates the p-value result, where darker colors are more significant.

Table 1. Metadata for all samples used in the statistical analysis of 18S rRNA gene amplicon survey, including year, maximum temperature (°C) at time of collection, concentration of microorganisms (cells ml^{-1}), estimated percent seawater in diffuse fluids (%), pH, magnesium (Mg mmol/L or mM), dissolved hydrogen (H_2 µmol/L or µM), total dissolved hydrogen sulfide

(H_2S mmol/L or mM), and methane (CH_4 µmol/L or µM). Values were taken from the most representative vent fluid measurements for each sample. Bags of vent fluid collected at depth and brought shipboard for filtering were sampled for geochemistry. For filters collected *in situ*, measurements from the most representative geochemistry sample were used. See materials and methods for more details.

Table 2. Summary of most frequently co-occurring ASVs. Table S4 lists all significantly co-occurring ASVs. Significantly co-occurring ASV interactions were dominated by the main protistan lineages listed in the first column. The other columns list the most common class, genus, or species level observed, the commonly co-occurring phyla, and information on inferred interaction type. Phagotrophy (or heterotrophy) is meant to describe protistan cells capable of engulfment (either passively hunting or actively seeking out prey) of microbial prey cells, while 'myzocytosis' is defined as "cellular vampirism" (Ramond *et al.*, 2019; Leander, 2020). Sources and examples of functional traits are listed as references (Moreira, 2003; Lima-Mendez *et al.*, 2015; Canals *et al.*, 2020; Schoenle *et al.*, 2020; Biard, 2022; Hess and Suthaus, 2022)

Table S1. Post quality control total number of sequences and ASVs for each sample included in the 18S rRNA gene sequence survey.

Table S2. Total number of ASVs and sequences, and sequence percentages by vent field, sample type, and all data, by major protistan taxonomic groups classified.

Table S3. Total number of ASVs or OTUs and percentage of ASVs or OTUs with respect to distribution (columns) and sequence dataset (rows). Results show consistent proportions of OTU distribution when ASVs are clustered at 99%, 97%, and 95% sequence similarity.

Table S4. List of significantly co-occurring ASVs derived from the SPIEC-EASI network analysis (Kurtz *et al.*, 2015). ASV-ASV co-occurrences are differentiated by "sideA" and "sideB", where this table first lists the sideA and sideB ASV feature IDs that co-occur.

V

	Year	Temperature (°C)	Microbial concentration (cells/mL)
Axial - Vent			
Dependable	2013	50	1.70×10^5
Marker113	2013	24.8	4.60×10^5
Marker113	2014	24.3	6.80×10^5
Marker113	2015	25.4	1.50×10^6
Skadi	2013	35.6	5.65×10^5
Escargot	2014	6.6	*nd*
El Guapo	2013	25.7	1.68×10^5
Boca	2013	6.8	8.50×10^5
Anemone	2013	28.2	4.10×10^5
Marker33	2013	27.3	4.20×10^5
Marker33	2014	18.5	3.90×10^5
N3Area	2013	18.9	2.57×10^5
Axial - Plume			
Anemone Plume	2015	*nd*	*nd*
Axial - Background			
Deep seawater	2015	2	2.50×10^4
GordaRidge - Vent			
Mt Edwards	2019	40	5.14×10^4
Venti Latte	2019	11	1.11×10^5
Candelabra	2019	79	5.51×10^4
Sir Ventsalot	2019	72	5.30×10^4
GordaRidge - Plume			
Mt Edwards Plume	2019	1.8	*nd*
Candelabra Plume	2019	1.7	7.69×10^4
GordaRidge - Background			
Deep seawater	2019	1.8	3.91×10^4
Shallow seawater	2019	8.6	*nd*
Near vent BW	2019	1.7	5.20×10^4
VonDamm - Vent			
X-18	2020	48	1.11×10^5
Shrimp Hole	2020	21	*nd*

Mustard Stand	2020	108	5.67×10^4
Ravelin #2	2020	94	*nd*
Old Man Tree	2020	121.6	*nd*
Ravelin #2	2020	98.2	*nd*
Arrow Loop	2020	137	1.04×10^4
White Castle	2020	108	*nd*
Bartizan	2020	129	1.62×10^4
VonDamm - Plume			
Plume	2020	4.2	1.65×10^4
VonDamm - Background			
Deep seawater	2020	4.2	3.47×10^4
Piccard - Vent			
Shrimpocalypse	2020	85	2.39×10^5
Lots O Shrimp	2020	19	5.39×10^4
Lots O Shrimp	2020	36	5.39×10^4
Piccard - Plume			
Plume	2020	4.5	5.14×10^4
Piccard - Background			
Deep seawater	2020	4.5	1.19×10^4

nd indicates no data available

bd indicates below detection

ent fluid parameters

Percent Seawater	CH4 µmol/L (µM)	pH	Mg mmol/L (mM)	H2 µmol/L (µM)	H2S mmol/L (mM)
90%	21	6.2	48.4	0.3	0.016
96%	17	6.2	51.5	1.4	0.75
96%	39	5.8	50.0	1.0	0.57
96%	23	6.6	51.4	0.3	0.59
90%	4.5	6.2	48.7	1.0	0.087
97%	2.1	5.8	52.6	0.047	0.035
92%	2.9	5.4	49.8	0.3	0.22
98%	1.6	6.9	53.0	2.8	0.0077
89%	15	5.5	47.6	14	1.1
87%	19	5.5	47.0	1.5	0.56
91%	6.6	5.6	49.2	1.5	0.27
98%	66	5.0	53.0	0.053	0.51
100%	*nd*	*nd*	*nd*	*nd*	*nd*
100%	0.002	7.8	53.6	0.002	0.0
83%	10	6.0	43.6	130	1.0
97%	0.9	6.4	52.1	*bd*	*nd*
88%	24	5.5	36.5	22	*nd*
98%	*nd*	*nd*	52.0	*nd*	*nd*
100%	*nd*	*nd*	*nd*	*nd*	*nd*
100%	*nd*	*nd*	*nd*	*nd*	*nd*
100%	*nd*	7.8	53.0	*nd*	*nd*
100%	*nd*	*nd*	53.0	*nd*	*nd*
100%	*nd*	7.8	53.0	*nd*	*nd*
52%	1,300	7.0	28.0	*nd*	2.1
96%	220	7.7	51.8	5.5	*nd*

36%	1,800	5.6	19.4	9,800	1.8
33%	1,900	5.8	18.0	10,000	1.4
26%	2,000	5.7	13.7	12,000	1.8
33%	1,900	5.8	18.0	10,000	1.4
34%	1,900	5.7	18.1	12,000	1.7
17%	2,300	5.5	8.9	14,000	2.0
42%	1,600	5.8	22.7	9,400	1.6
100%	*nd*	*nd*	*nd*	*nd*	*nd*
100%	*nd*	*nd*	*nd*	*nd*	*nd*
82%	28	5.1	43.9	0.0	*nd*
100%	12	6.3	53.5	1.3	*nd*
95%	11	5.9	51.0	23,000	*nd*
nd	*nd*	*nd*	*nd*	*nd*	*nd*
100%	*nd*	*nd*	53.7	*nd*	*nd*

	Location	
Depth (m)	Latitude	Longitude
1,913	45.8799	-129.8029
1,520	45.9227	-129.9882
1,518	45.9227	-129.9882
1,520	45.9227	-129.9882
1,562	45.9234	-129.9829
1,517	45.9264	-129.9791
1,502	45.9266	-129.9795
1,517	45.9277	-129.9825
1,542	45.9332	-130.0137
1,516	45.9332	-129.9822
1,514	45.9332	-129.9822
1,523	45.9437	-129.9852
1,500	45.9336	-130.0137
1,520	46.2739	-129.7955
2,707	42.7546	-126.709
2,708	42.7548	-126.7089
2,730	42.7551	-126.7096
2,732	42.7612	-126.7055
2,707	42.7547	-126.7092
2,725	42.7551	-126.7094
2,010	42.7495	-126.7103
150	42.7546	-126.743
2,745	42.755	-126.7099
2,377	18.3748	-81.7974
2,376	18.3749	-81.7974

2,374	18.3751	-81.7975
2,390	18.3751	-81.7972
2,376	18.3751	-81.7977
2,389	18.3751	-81.7972
2,309	18.3767	-81.798
2,307	18.377	-81.7981
2,307	18.7981	-81.3779
1,979	18.3776	-81.7993
2,400	18.3742	-81.7815
4,945	18.5467	-81.7178
4,967	18.5468	-81.7184
4,967	18.5468	-81.7184
4,944	18.5468	-81.7182
4,776	18.548	-81.7182

Group	Common taxa found significantly co-ocurring in this study	Frequently co-occur with phyla
Cercozoa	*Filosa-Thecofilosea;Ventricleftida, Endomyxa;Vampyrellida, Endomyxa; Endo4-lineage*	Ciliates, dinoflagellates, other cerocozoa
Ciliates	*Plagiopylea, Nassophorea;Discotrichidae, Phyllopharyngea; Cyrtophoria, Scuticociliatia;Philasteria*	Other ciliates, haptophytes, dinoflagellates, and cerocozoa
Dinoflagellates	*Dino-Group-III, unclassified Dinophyceae, Dino-group-I (clade 5)*	Haptophytes, other dinoflagelaltes, ciliates
Haptophytes	*Chrysochromulina spp., Prymnesiophyceae*	Other haptophytes, Dinophyceae
Opalozoa, Pseudofungi	*Bicoecea; Anoeca (Anoeca_atlantica), MAST-3I, MAST1B*	Other stramenopiles, Dinophyceae, ciliates
Radiolaria	*Astrosphaeridae;Heliosphaera, RAD-C, -B*	Dinoflagellates, haptophytes

Inferred nutritional strategy	Specialized interaction	Morphology & motility characteristics
Parasitic to other eukaryotes, or an active or passive phagotroph	Cercozoa include generalist predators, that may exclusively consume eukaryotes, predatory amoebae, or can be parasitic to fungi.	Amoeboid or elongated cell morphology, typically capable of gliding or swimming
Phagotrophy or myzocytosis. Predation by passive or active feeding	Preferred prey will be other protists, ciliates, and bacteria; includes parasitic lifestyle, and anaerobic species	Typically round or elongated cell structure and moves as swimmer or in gliding motion
Phagotrophy or myzocytosis; Passive or active ambush predator	Syndiniales are parasitic to metazoan larval stages, mollusca, other protists (especially dinoflagellates). Other uncalssified Dinophyceae may be are predators to other protists and bacteria	Naked, round cell shape, typically swimming motility, while parasitic species live attached to hosts
Phagotrophy, active ambush feeder	Known as a globally-distributed mixotroph; at vent environment, assumed to be primarily heterotrophic	Round, flagellated, swimming cells
Phagotrophy; active ambush feeder or cruise feeder	MAST typically bacterivors, while Bicoecea may be less specialized	Naked, round cell that moves in gliding or swimming manner
Phagotrophy; active or passive feeding	Often host to dinoflagelalte or haptophyte symbionts; pseuopodial networks to capture prey	Silliceous or strontium sulfate cell structure, round or amoeboid; planktonic

References
Hess & Suthaus 2022
Lynn, 2008; Canals et al. 2020
Moreira & Lopez-Garcia 2003; Lima-Mendez et al. 2015
Hansen and Hjorth 2002
Schoenle et al. 2020
Biard et al. 2022

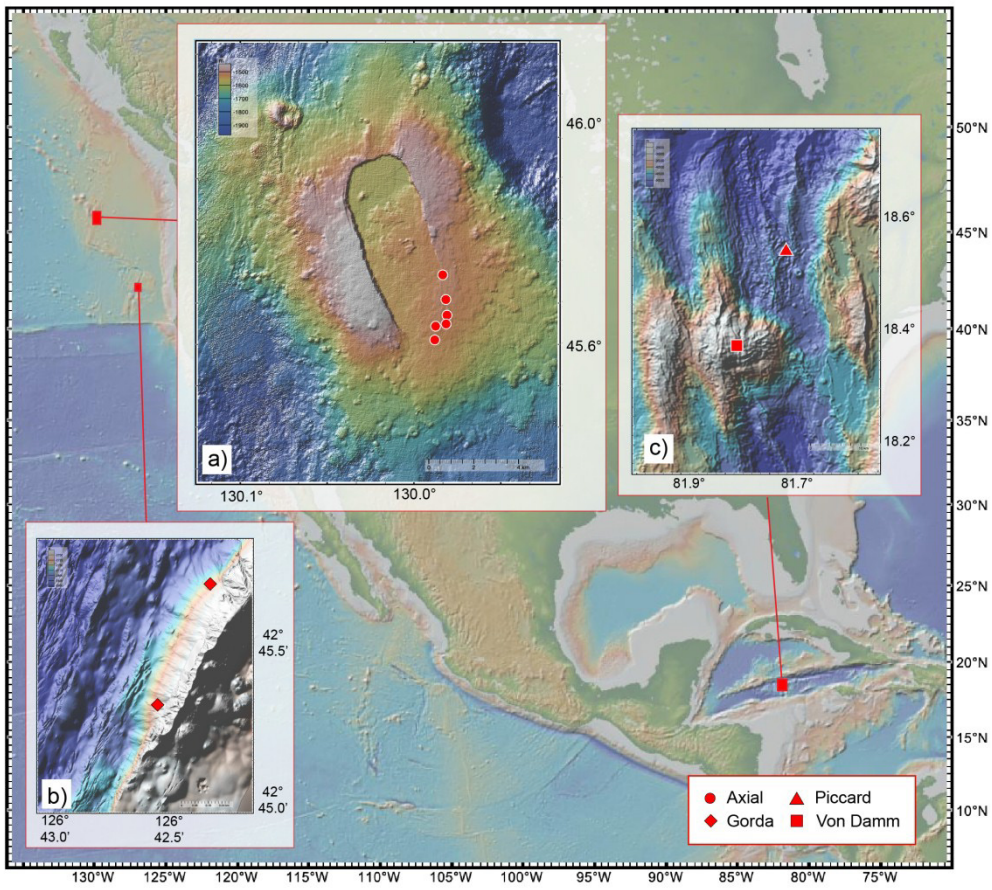

Figure 1. Map of all vent fields, where symbols represent each vent site at Axial Seamount (a), (b) the two regions sampled at the Gorda Ridge, and (c) the Piccard and Von Damm vent fields along the Mid-Cayman Rise. Figure made with GeoMapApp (www.geomapapp.org) / CC BY / CC BY (Ryan et al., 2009).

780x733mm (72 x 72 DPI)

Figure 2.

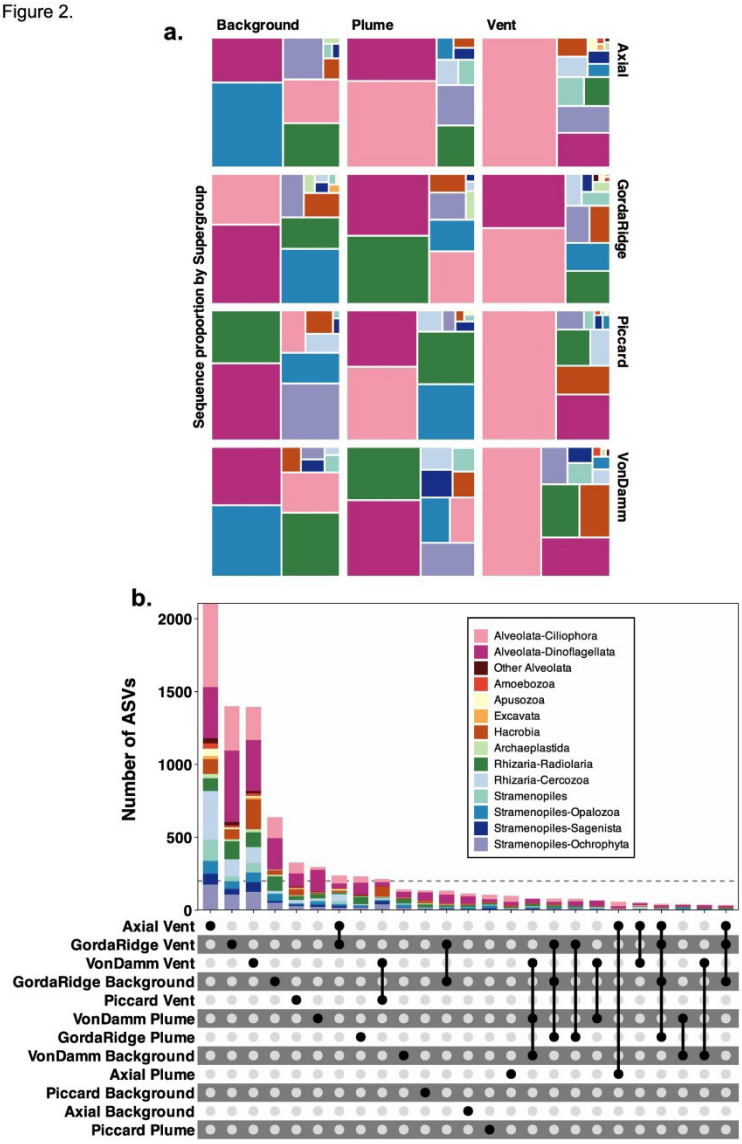

Figure 2. (a) Proportion of sequences belonging to main protistan supergroup and phyla, by sample type (left to right: Background, Plume, and Vent) and hydrothermal vent field (top to bottom: Axial Seamount, Gorda Ridge, Piccard, and Von Damm. ASVs with fewer than 200 sequences were removed. (b) Total number of shared (or unique) ASVs across sample type and vent field. Dot matrix below the bar plot indicates the samples included in the bar plot representation, where the bar plots above a single dot indicate that those ASVs were restricted to that vent field and sample type. Colors represent main protistan taxonomic groups. Dashed line indicates 200 ASVs were shared (y-axis); Figure S3 includes a comparison of samples with <200 ASVs.

215x279mm (300 x 300 DPI)

Figure 3.

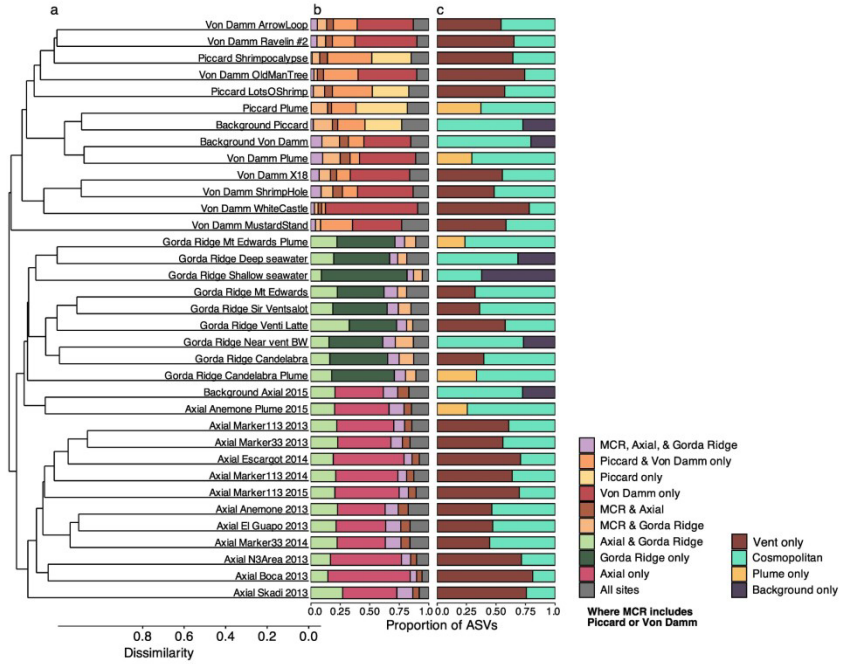

Figure 3. (a) Community diversity clustered by Jaccard Dissimilarity, where values closer to 0 indicate samples are identical. (b) Proportion of ASVs shown by distribution among hydrothermal vent sites, Axial, Gorda Ridge, Piccard, and Von Damm (where Mid-Cayman Rise is abbreviated MCR and includes Piccard and/or Von Damm). (c) Proportion of ASVs designated as vent only (resident or putative endemic), cosmopolitan (found among background, plume, and diffuse vent fluid), plume only, or background only.

215x279mm (300 x 300 DPI)

Figure 4.

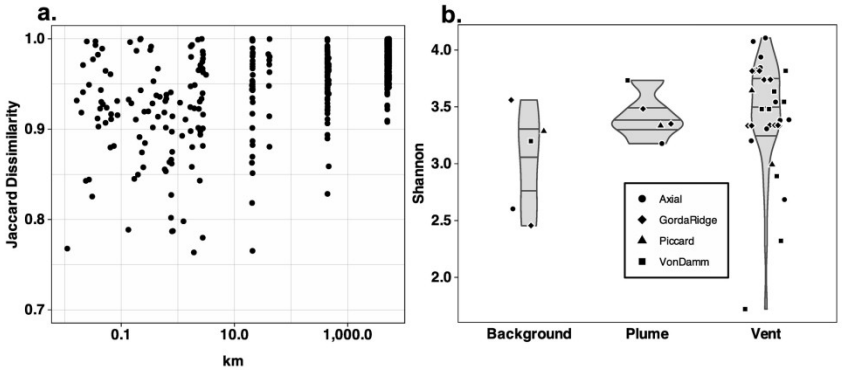

Figure 4. (a) Distance-decay plot, where data points represent pairwise comparisons of all samples (Distance-decay with resident and cosmopolitan populations can be found in Figure S4), and distance between the samples is represented on the x-axis with the community dissimilarity (estimated by Jaccard) is represented along the y-axis. Comparison of Jaccard distance variance to geographic distance is also reported in Figure S4. Note that geographic distances represent the calculated difference between latitude and longitude (Table 1), rather than oceanographic distances. (b) Violin plot of estimated Shannon values (derived from DivNet), by sample type (x-axis), background, plume, and vent site.

215x279mm (300 x 300 DPI)

Figure 5.

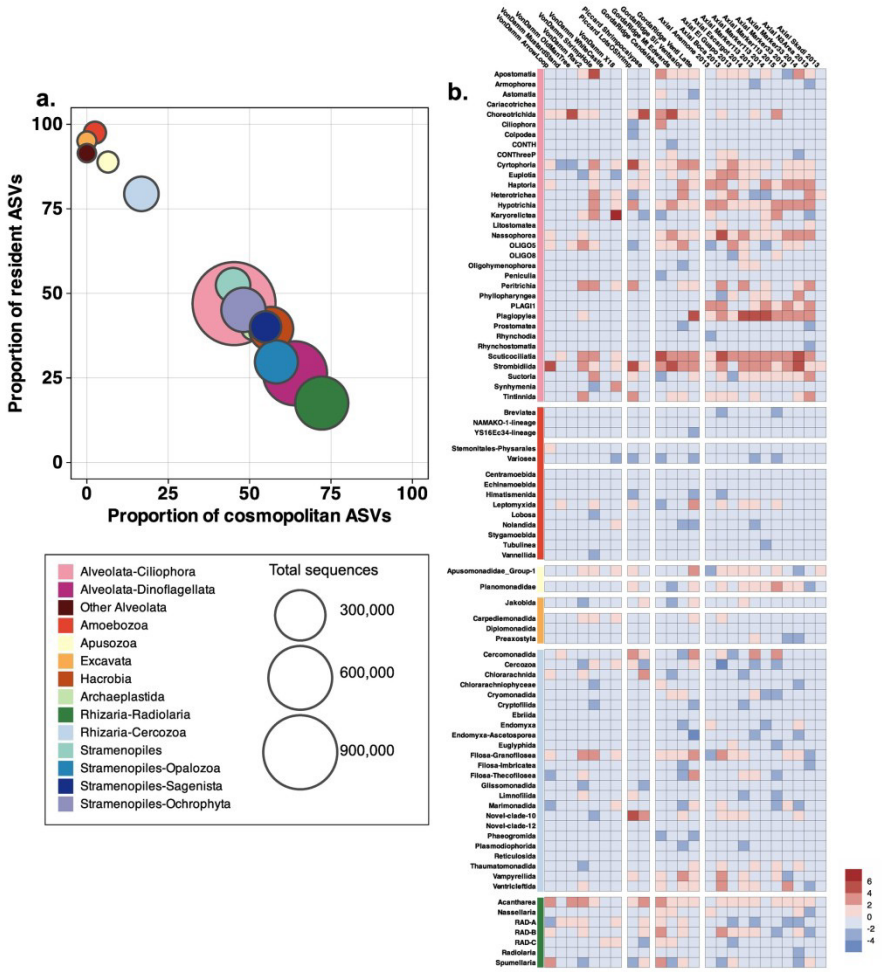

Figure 5. (a) Relative proportion of ASVs classified as resident (y-axis) versus cosmopolitan (x-axis). Bubble size is equivalent to the total number of sequences and color represents each supergroup. (b) Vent-only (putative endemic) taxa represented by CLR transformed data (red to blue) by vent sample (x-axis) and taxonomic class (y-axis). Sum of CLR transformed data will equal 0, where the log of the ratio between each data point at the geometric mean of the dataset is calculated.

215x279mm (300 x 300 DPI)